Research Article

Mediterranean Marine Science
Indexed in WoS (Web of Science, ISI Thomson) and SCOPUS
www.hcmr.gr
DOI: https://doi.org/10.12681/mms.43030

Multi-decadal assessment of shoreline changes and future response along the Acheloos river delta, Greece

Stelios PETRAKIS[1,2], Emmanuel VASSILAKIS[2], Serafim POULOS[2] and Vasilios KAPSIMALIS[1]

[1] Institute of Oceanography, Hellenic Centre for Marine Research, 46.7 km Athens-Sounio Ave., Anavyssos 19013, Greece
[2] Faculty of Geology and Geoenvironment, School of Science, National and Kapodistrian University of Athens, University Campus, Zografou 15784, Greece

Corresponding author: Stelios PETRAKIS; s.petrakis@hcmr.gr

Contributing Editor: Stelios SOMARAKIS

Received: 20 October 2025; Accepted: 18 January 2026; Published online: 20 April 2026

Abstract

The present study investigates alterations in the coastal area of the Acheloos deltaic complex (W. Greece) during the period 1945 – 2020 and the shoreline response to anticipated sea-level rise under various RCP scenarios. The authors used two methods of analysis: area measurement in non-linear sections of the coast, and longitudinal displacement of the coastline using DSAS. The future state of the coastal area analyzed by considering IPCC predictions, adjusted for local conditions. The results reveal severe erosion in the entire study area, reaching 250 m (~3.4 m/yr) in places, mostly due to the diversion of the main Acheloos River channel, whereas coastal protection works constructed in the 90s have partially mitigated the erosional rate. The IPCC predictions for 2100 show a continuous shrinking of the delta by 10% to 20% of the present area, while under the most extreme climate scenario, deltaic area loss could reach 60%. Regardless of the prevailing scenario, it was estimated that for each 0.1 m of sea-level rise, the average land loss at the deltaic area is approximately 2.8 km^2.

Keywords: Delta evolution; shoreline change; coastal geomorphology; DSAS.

Introduction

River deltas are areas of great socioeconomic importance, as they provide habitat for a large number of species of flora and fauna, while due to their morphology they are suitable for settlement, agricultural, industrial and tourism. Also, the submerged deltaic area may also contain exploitable aggregate reserves due to delta formation processes.

According to (Cazcarro *et al.*, 2018), it has been estimated that of the approximately 2.5 billion people who currently live in direct contact to the coastal areas (41% of the world's population), 500 million (1/10 of the world's population) live in deltaic areas. This is mainly due to the euphoria of the deltaıc sediment, the possibility of relatively easy management of deltaic areas, the gentle topography and the development of riverine trade routes (Karymbalis, 2010).

At the drainage basin scale, flood control works, dams for hydropower, irrigation and watering, the dredging of channels for the extraction of aggregates lead to a disconnection of the delta from its upstream area, depriving it of river sediment (Dunn *et al.*, 2019; Kapsimalis *et al.*, 2005; Schmitt *et al.*, 2018). In a global scale, Vörösmarty *et al.* (2003) estimated that since 1985, 30% of the sediment that would normally end up in the delta mouths is trapped along the riverbed, behind dams, with a direct result of more rapid subsidence of the deltaic plains, (Parcharidis *et al.*, 2013), the degradation of coastal wetlands and ultimately the increase in the shoreline retreat rates at the coastal area. Syvitski *et al.* (2022) increased that percentage to 49% for the last 60 years, whilst adding that the overall societal consumption of sediment for the same period has increased by 2,500%.

Within deltaic plains, human activities cause local effects such as subsidence due to extraction of groundwater and hydrocarbons, land drainage, and construction (Syvitski *et al.*, 2009). Exploitation of deltas to yield social and economic benefits has led to many deltas becoming "locked-in" to states of high risk (Santos & Dekker, 2020) and costly, rigid, and energy-intensive adaptation strategies (e.g., the Dutch Delta Works).

Furthermore, the ongoing climate change (and/or variability) has been identified as a contributing factor to the significant loss of deltaic plains, as reported in the IPCC 6th Assessment Report (Calvin *et al.*, 2023) and by Scown *et al.* (2023). This loss is attributed to changes in sea level rise and variations in storm intensity and frequency (e.g., Alley *et al.*, 2005). Meyer & Peters (2016)

estimate that due to increasing flooding in deltaic areas, by 2100 more than 100 million people will have been compelled to relocate from such areas, with the consequent impact on the global economy.

It is evident that socio-economic activities in many deltas have become disconnected from the ecosystems upon which they fundamentally rely (Reader *et al.*, 2022); this disconnection is frequently accompanied by negative feedback on ecosystem services (Vörösmarty *et al.*, 2009; Ludwig *et al.*, 2010). Thus, Integrated Coastal Zone Management (ICZM) through models such as DPSIR (Elliott, 2002); (Kristensen, 2004), especially in recent years, is an integral part of the strategy at local, national and global levels.

In the Mediterranean, an equally significant loss is observed in the coastal area of the most important deltas (Anthony *et al.*, 2021, 2017; Besset *et al.*, 2019, 2017). In Greece particularly, the construction of dams at the larger rivers (e.g., Nestos, Evros, Evinos, Alfios and Pinios) has doubled or even tripled the erosional rates at the deltaic coastal area (Andredaki *et al.*, 2014; Ghionis *et al.*, 2013; Karditsa *et al.*, 2020; Karymbalis *et al.*, 2022, 2016; Poulos, 2019; Poulos *et al.*, 2002).

The present study has a twofold scope. Firstly, it aims to quantify the Acheloos delta's lost area over the past 75 years, taking into consideration the construction of dams and the presence of coastal protection structures, and secondly, to provide estimates for future land loss due to the ongoing sea level rise induced by climate change.

Study Area

The delta of Acheloos river is one of the largest in Western Greece, having an area of about 270 km^2 and is generally characterized by very gentle (to almost zero) slopes. Figure 1 depicts the geomorphology of the area and its associated systems, as they have been superimposed over the digitized topographic diagrams from the Hellenic Military Geographical Service. The deltaic plain, at the last 10 km of the main river channel, has an altitude span of less than 4 m, while the hills of the area (Dioni, Skoupas, etc.) have an altitude that does not exceed 180 m, with the exception of Koutsilari hill in Southern part, whose altitude reaches up to 420 m. The low relief of the area is the main reason for the frequent alteration of the Acheloos River main bed over the years, a fact supported by the existence of many abandoned channels, on either side of the main bed, scattered at the deltaic plain. Where sand supply is limited, the coastline is marked by a sandy low-tide terrace, and a berm or storm ridge built of variable proportions of sand and reeds. Only near delta mouths is sand supply sufficient for broad barrier beach-dune systems to form. At its southern area there are extensive marshes, which are partially controlled by constructions.

The coastal front consists of two distinctive parts: (i) the western delta having clay-sandy coasts shaped by the combined action of waves and tides; and (ii) the southern part, including the river mouth, formed by sandy beaches along with submerged bars and a complex pattern composed by

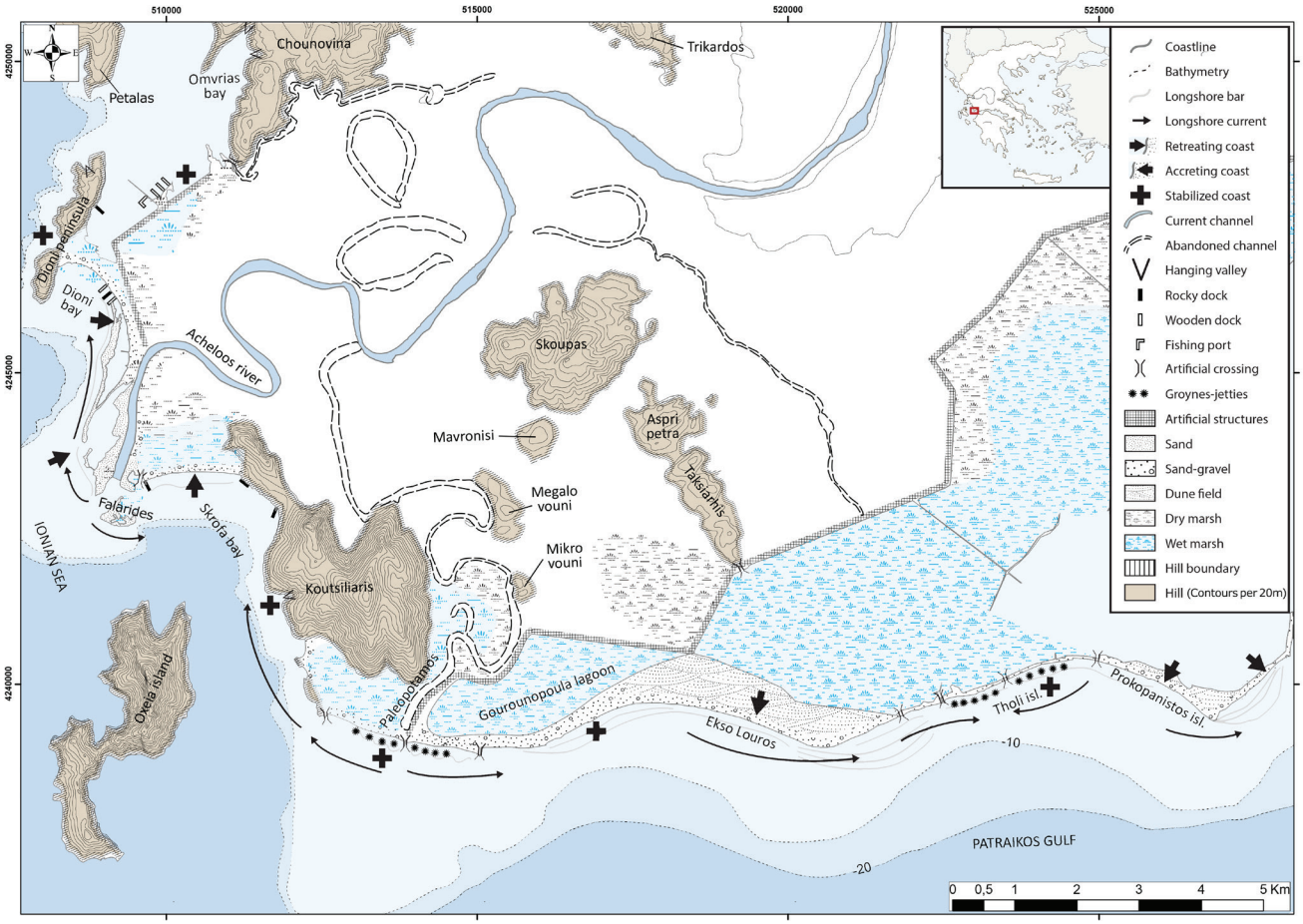

Fig. 1: Geomorphologic map of the Acheloos deltaic area and toponyms referred to in the paper.

berms and a beach-dune ridge (Tzanetatou *et al.*, 2002).

The underwater morphology of the NE and E side of the Inner Ionian has been formed mainly due to the sedimentological processes of the Acheloos River estuaries (Fig. 2). The map was generated through the integration of depth records from the HCMR archive and bathymetric survey data collected in 2018. The subaqueous prolongation of the deltaic plain extends from the shoreline to a depth of about 10 m, along the deltaic shoreline, in variable widths up to 2 km. The underwater deltaic front is distinct, due to the sharp alteration in the bottom slope at depths of 15 to 30 m.

The oceanographic conditions of the broader area follow the average conditions of the Ionian Sea (Soukisian *et al.*, 2007), with average annual significant wave height (H_s) between 0.3 and 0.6 m and average annual significant wave period (T_s) between 4.8 and 5.6 sec, rather low, since the area is fortified by the large Ionian Islands. The average annual wind speed (U_w) ranges between 2 and 3 m/sec, with wind speeds of over 11 m/s being observed with frequency <4%. The tidal regime is very low, with a tidal range of 0.86 m (Hydrographic Service - Hellenic Navy, 2015).

Human activity such as fisheries and agriculture is very common in the area, while six hydroelectric dams control the river flow. Moreover, coastal works support the barrier islands and the associated lagoon and marsh areas that are used in aquaculture.

The catchment area of the Acheloos River extends in a North-South direction (Fig. 3). Covering a total area of approximately 7530 km^2, it is the 6th largest watershed in Greece, while it is second largest, compared to the rivers of which their whole watershed is located in the Greek territory. Geologically, the basin area belongs to the Ionian and Gavrovo Zones, with Post-Alpine (Quaternary) sedimentary formations and Molasses (Papanikolaou, 2015). In the southernmost part, the entire area is covered by Plio-Pleistocene deposits.

The study of the Acheloos delta complex through 3D seismic reflection data that captures the entire deltaic body constitutes an example of the evolution of a fluvial-dominated delta of Pleistocene age in a confined setting, affected by tectonic events followed by salt diapirism (Lykakis *et al.*, 2021; Stathopoulou *et al.*, 2023; Underhill, 1988). It is worth mentioning that no evaporite lithologies (halite, gypsum) have been identified in the deltaic surface or upper stratigraphy (Soto *et al.*, 2024).

The mean annual water discharge (prior to damming) reached the 8 km^3 the suspended sediment load 3.3x10^6 tones and the dissolved load (1.5x10^6 tones) (Milliman & Farnsworth, 2011; Poulos & Collins, 2002; Skoulikidis, 2018). Figure 4 presents the available data of water and sediment discharges in association with the presence of the 6 hydroelectric dams, superimposed on top of the precipitation records for the years 1955-2005, period in which the aforementioned data is available.

The modern type of the Acheloos delta (according to Galloway, 1975) tends to acquire the characteristics of a delta in which wave processes dominate, despite its previous type as a fluvial dominated delta, as wave conditions now play a major role in shaping the morphology of the area, due to the dramatic reduction in sediment yield and essentially through the redistribution of pre-existing sediments on either side of the estuaries, with the formation of sandy barriers and underwater ridges.

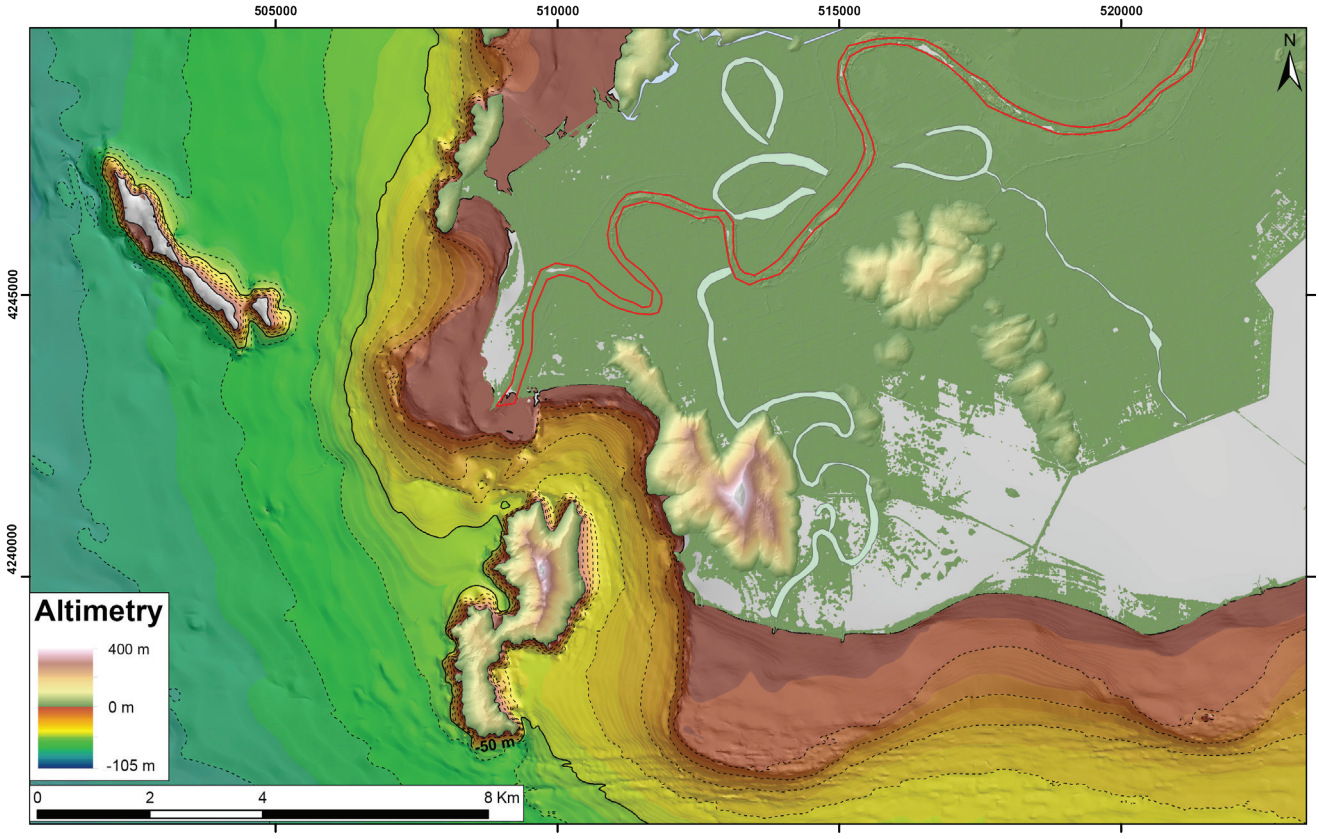

Fig. 2: Underwater morphology of the Acheloos deltaic area.

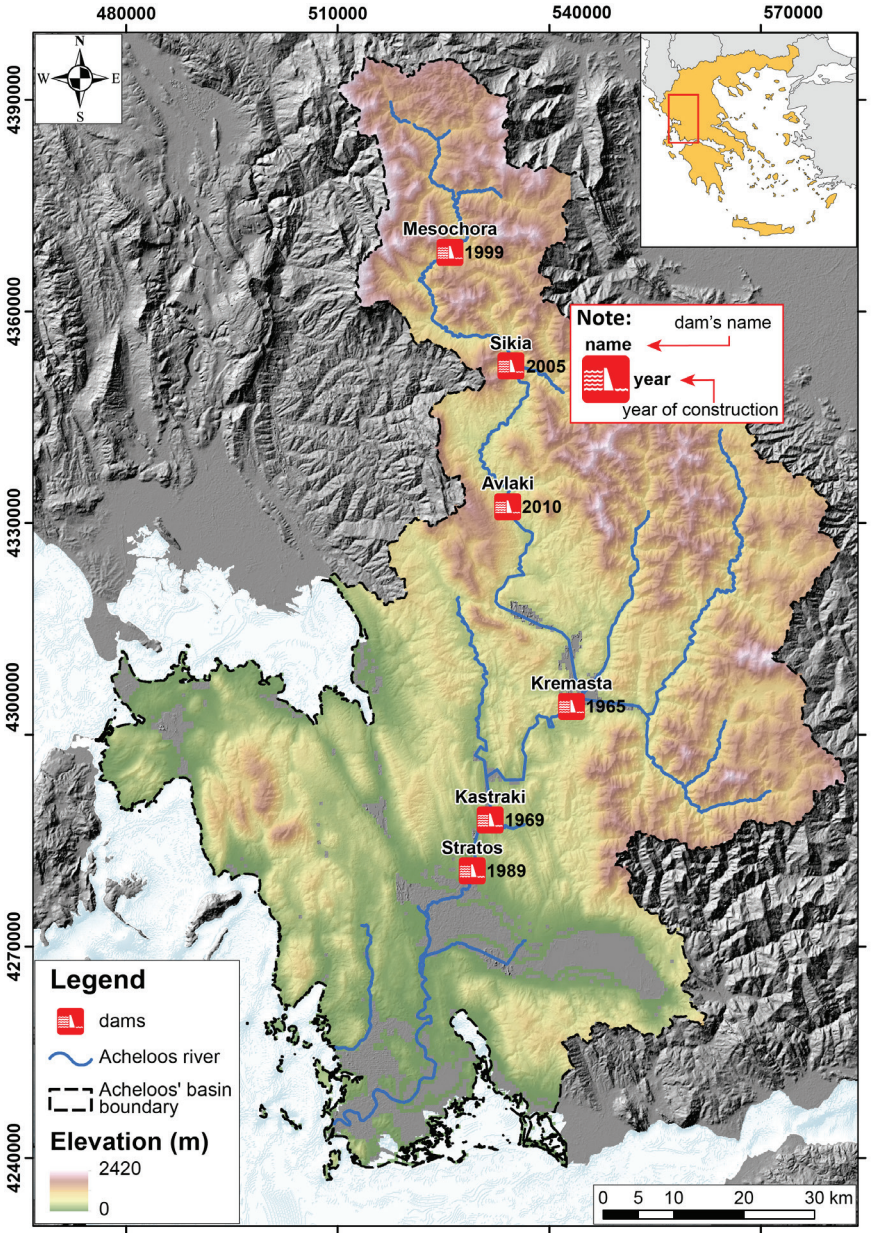

Fig. 3: Geomorphologic map of the Acheloos drainage area.

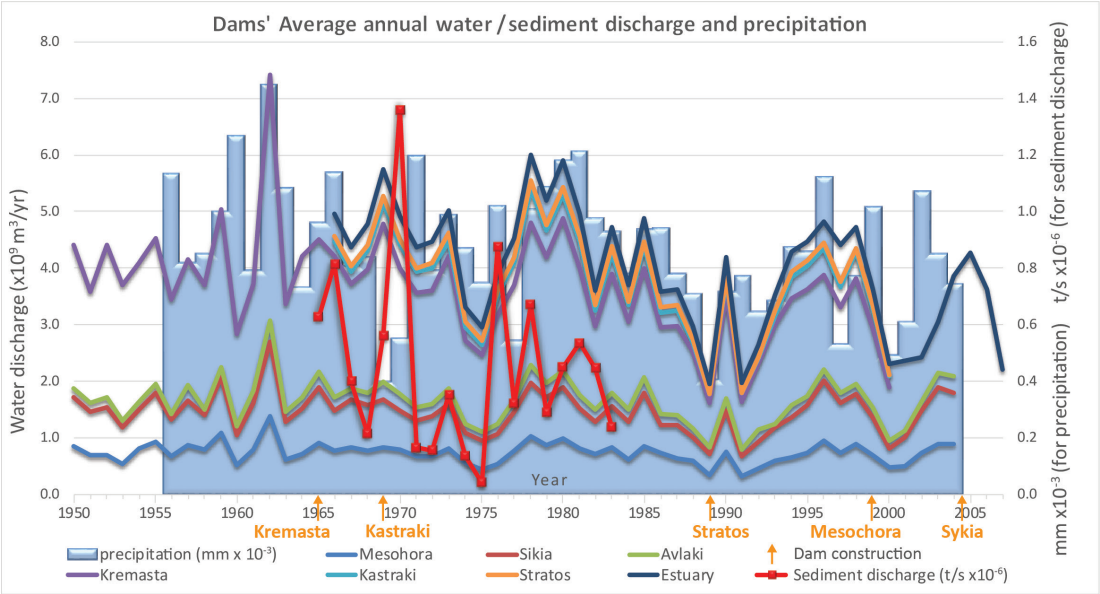

Fig. 4: Annual water – sediment discharge at the route measure points.

Materials and Methods

Study of the coastal area alteration through time

The broader area of the Acheloos River delta front is a quite complex morphological site in which the border between land and sea is constantly changing, mainly due to the very low relief of the coastal area. As a result, there are common phenomena of ephemeral floodings of areas that were previously above sea level and vice-versa, merges or separations of islets, continuous natural changes of sediment budget volumes, as well as construction of coastal works for the protection of this sensitive area from the waves' action. The aforementioned alterations require the study of the overtime change of the coastal area by sections and not as a whole area, using available aerial photographs and satellite images. Two methods of analysis were chosen: (a) area measurement, in the areas where the coastline is not linear and there are often floodings and draining of large sections, and (b) longitudinal displacement of the shoreline through the DSAS (Digital Shoreline Analysis System) software, a dedicated sub-routine of the ArcGIS 10.8 software (Himmelstoss *et al.*, 2018), in areas where the shoreline is relatively linear and displacements are observed on a relatively parallel axis during the last 75 years. Dsas has been frequently used in similar cases (Guneroglu, 2015; Nghiningwa *et al.*, 2025; Ortega *et al.*, 2023; Rafi *et al.*, 2024; Tsokos *et al.*, 2018), providing accurate outcomes, and, most importantly, shining light to the areas with the most pressure. The following characteristics were calculated in each study sub-area:

- Net Shoreline Movement (NSM) which refers to the distance between the newest and the oldest digitized shorelines for each transect, measured in meters.
- End Point Rate (EPR) of each transect, which refers to the NSM divided by the years between the oldest and the most recent shoreline, measured in m/yr.
- Finally, the total area displacement of each section was calculated for the last 75 years.

In Figure 5 the areas in which the first method was applied are presented in a yellow box ([a] – estuary lobe and [b] – elongated islets) and in an orange box the areas in which the second method was applied ([1] – Scrofa beach, [2] – Paleopotamos and Ekso Louros beaches, [3] – elongated islet of Tholi and [4] – elongated islet of Prokopanistos).

A total of 70 images were used, covering the period 1945 – 2020, of which 51 were aerial photographs from the Hellenic Military Geographical Service (H.M.G.S.), of various scales and resolutions, and 19 were satellite images from Planet Labs Inc, a free satellite imagery hub. The aerial photographs were scanned in a high-resolution scanner (800-1200 dpi), while all images were processed in a GIS software. They were georeferenced to a WGS 84 / UTM zone 34N coordinate system, based on control points, scattered throughout the study area. Subsequently, the coastlines of all corresponding dates were digitized and depending on the area, the aforementioned analyses were applied. The details of the images used are presented in Table 1.

Study of the sea level rise rates

To predict the land loss of the study area until the year 2100, an analysis of the existing situation was performed and the predictive models of the Intergovernmental Panel on Climate Change (IPCC) were applied to the area (Pörtner *et al.*, 2019).

According to the study by (Jevrejeva *et al.*, 2016), a grid has been constructed with a distance of one degree (1°) per point of intersection, which covers the whole earth, and on each point the predictions for the change of sea level per decade, from 2010 to 2100, considering the change scenarios RCP2.6 (very moderate scenario), RCP4.5 (moderate scenario), RCP8.5 (extreme scenario) and High-End RCP8.5 (extreme scenario) of IPCC (H.-

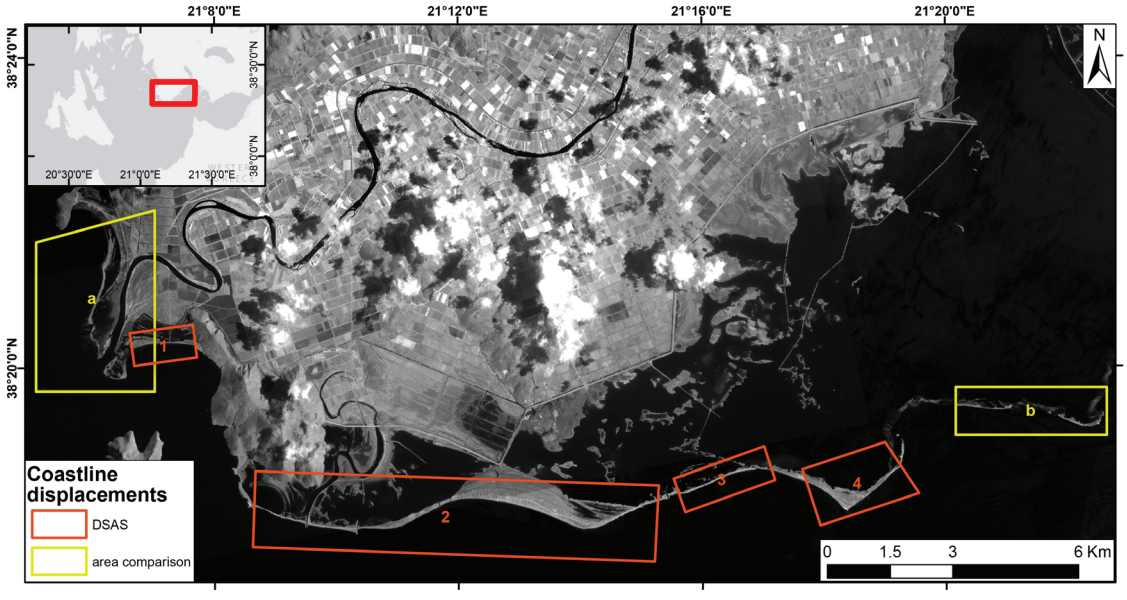

Fig. 5: Coastal alteration areas of analysis of the Acheloos broader area (Image © 2020 Planet Labs PBC).

Table 1. Index of aerial photos and satellite images used for the study of the evolution of the coastal Acheloos area.

Date	Type	Scale	Pixel size	Quantity	Source
31/08/1945	Aerial photo	1:42000	1.5 m	6	H.M.G.S.
1960	Aerial photo	1:30000	1 m	9	H.M.G.S.
1971	Aerial photo	1:40000	1.5 m	6	H.M.G.S.
16/06/1986	Aerial photo	1:40000	1.5 m	5	H.M.G.S.
24/06/1992	Aerial photo	1:8000	1 m	17	H.M.G.S.
06/11/1996	Aerial photo	1:40000	1 m	4	H.M.G.S.
23/08/2006	Aerial photo	1:40000	1.3 m	4	H.M.G.S.
06/05/2009	Satellite image	-	5 m	4	Planet Labs, Inc
16/07/2011	Satellite image	-	5 m	4	Planet Labs, Inc
12/06/2014	Satellite image	-	5 m	3	Planet Labs, Inc
04/06/2017	Satellite image	-	3 m	5	Planet Labs, Inc
04/06/2020	Satellite image	-	3 m	3	Planet Labs, Inc

O. Pörtner *et al.*, 2019). Also, the confidence intervals of 0.05, 0.17, 0.50, 0.84, 0.95 and 0.99 were calculated for each of the scenarios. For each scenario the 0.5 confidence interval was used, which is the average of all confidence intervals, as well as 0.05 and 0.99 for the construction of the visualization diagrams of the sea level change range.

The relevant to each aforementioned scenario flooding areas were calculated in GIS, based on the high resolution DTM of the broad area and "bathtub" methodology (NOAA, 2012) was used, with the assumption that all flooding coastal areas communicate with each other, due to the general very low relief.

Results and Discussion

Coastal zone displacement (1945 – 2020)

Area measurement

Acheloos estuary

For the area measurement of the Acheloos estuary, a control polygon was created, within which the area of the land was measured for all the years in which data were available (Fig. 6). The results are shown in Figure 7.

During the last 75 years (1945-2020), the estuary area has changed radically. Major changes are observed on the outer western side of the estuary, as well as on the Falarides islet that is forming east of the river mouth of the Acheloos main branch. The outer western side moves continuously to the north-east, in a relatively clockwise displacement, with simultaneous elongation of the sediments of the deltaic sandy arm (spit) to the north, in Dioni Cove, due to the transport of sediments in the same direction and the direction of coastal currents. The land west of the main river has been retreating continuously for the last 75 years, while no advance of the estuary is observed at all, as an indication of the reduced sediment supply of the river and the northward action of coastal currents.

At the same time, Falarides islet, the result of sediment accumulation which appears for the first time during the period 1960-1971, increases its size towards the northeast, having, in 2020, almost joined the eastern shore of the Acheloos estuary. The direction of transport and deposition of the sediments is from SW to NE, so that sediment arms are formed on either side of the islet, facing the opposite coastline.

Between 1996 and 2003, a 300 m long vertical groyne was constructed at the western part of Scrofa Bay, east of the current estuary, due to which sediment accumulated in its eastern area. Figure 6 also shows the displacement of the main route of Acheloos towards the north, during the period 1945-1971, while after 1971 its position seems to generally stabilize to its present area.

According to the area measurements of the various years, the dry part of the estuary in 1945 had an area of 3.934 km^2, which in 2020 had decreased to 3.241 km^2, with a total loss of about 0.7 km^2. According to the analysis (Fig. 7), erosion does not evolve linearly throughout this time period. From 1945 to 2009 the area of the estuary decreased continuously and progressively, relatively linearly, with an annual erosion of about 5000 m^2. The maximum total loss, based on the 2009 satellite image, was measured to be 0.82 km^2. From 2009 to 2020, a continuous linear accretion is observed, with an annual rate of about 15000 m^2 and a total land gain of 0.1 km^2, reaching the final balance of -0.7 km^2, which corresponds to about 20% of the total area measured.

It is worth noting that the eroded area, almost in its entirety, is located in the main lobe of the estuary, while the deposited area is located almost exclusively in the creation and enlargement of the islet south-east of the estuary, from 1971 onwards.

Elongated islands of Messolonghi lagoon

At the southern border of the Messolonghi lagoon are located, from west to east, the elongated islets of Schinia, Komma and Agios Sostis (Fig. 8). These islets are flattened in the E-W direction and constitute a split extension of the coast that includes Louros and Prokopanistos, located about 3 km to the NE.

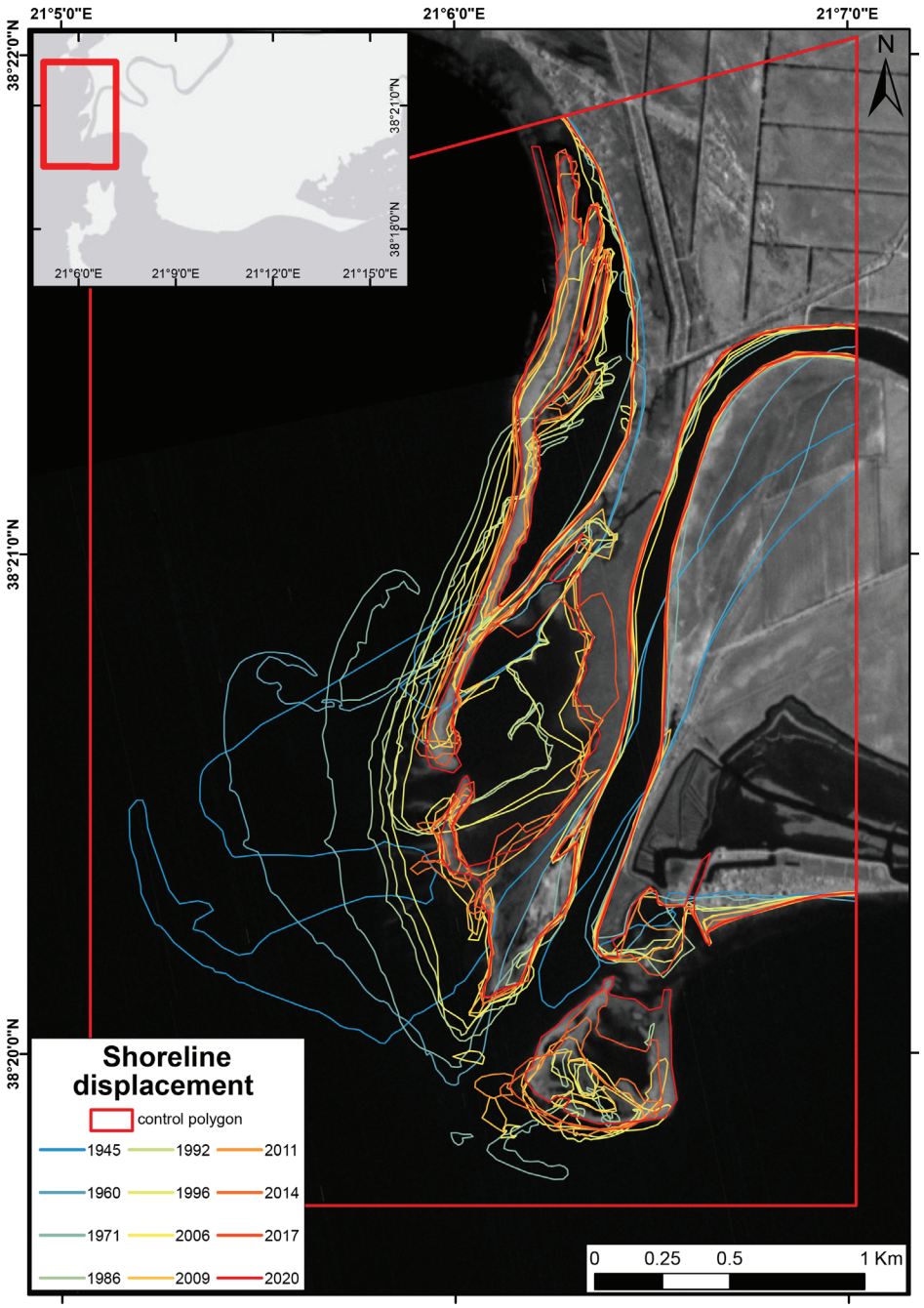

Fig. 6: Evolution of the Acheloos estuary during the period 1945-2020. The background satellite image is from 2020.

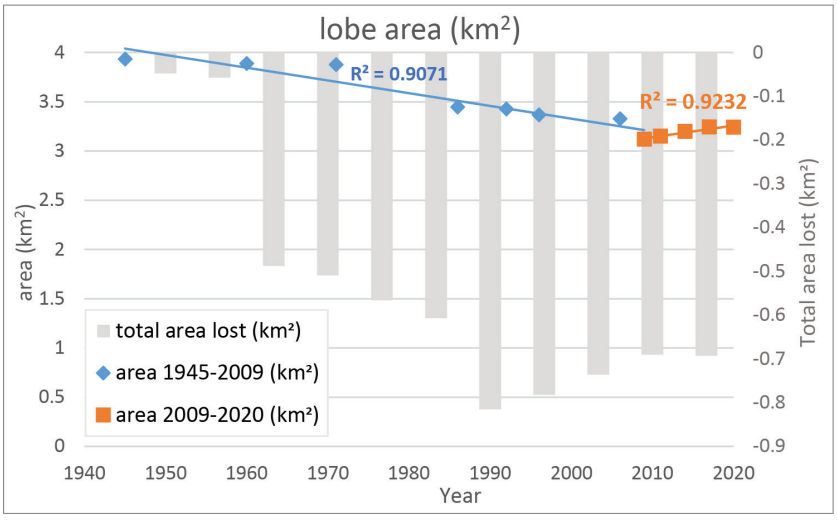

Fig. 7: Evolution of the active Acheloos estuary area during the period 1945-2020 (km^2)

In order to study the evolution of the islets' coastal are, the temporal change of their surface, during the last 75 years, was measured. The elongated shape of the islets, their small surface area, the absence of plants and man-made structures and the constant change of their boundaries made georeferencing difficult, but even in this case the georeferencing accuracy was less than 3 meters. Also, due to the existence of very small depths that, combined with the strong presence of algae and underwater structures for the demarcation of fish farms at the north part of the islets, the digitization of the coastline was performed with relative precision, by switching the brightness and alternating the spectral bands of the relevant aerial photographs and satellite images.

Shinias island

The islet of Shinias changed significantly during the period 1945-2020, mainly at its eastern part. As shown in Figure 9, the total surface loss in the last 75 years is 0.08 km^2, which corresponds to 40% of its original surface.

Komma and Ag. Sostis Islets

The islets of Komma and Ag. Sostis have also undergone significant morphological changes during the last 75 years. As shown in Figure 8, the islet of Komma joined with Ag. Sostis during the period 1945-1960, they remained tied until 2012, reducing their area throughout this period, while in 2013 they split again, reaching the current state in 2020. The eastern part of Ag. Sostis did not change significantly throughout this period, with the exception of its eastern edge, which lengthened slightly towards the North.

The total surface loss of the complex Komma – Ag. Sostis in the last 75 years is 0.02 km^2, which corresponds to 15.5% of its original surface (Fig. 10).

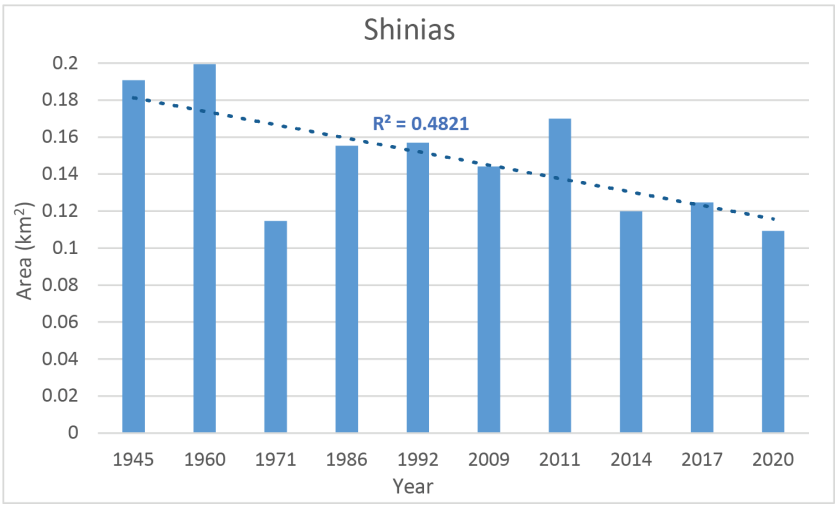

Fig. 8: Change of the islets' area, located at the southern part of the Messolonghi lagoon during the period 1945-2020. The background satellite image is from 2020.

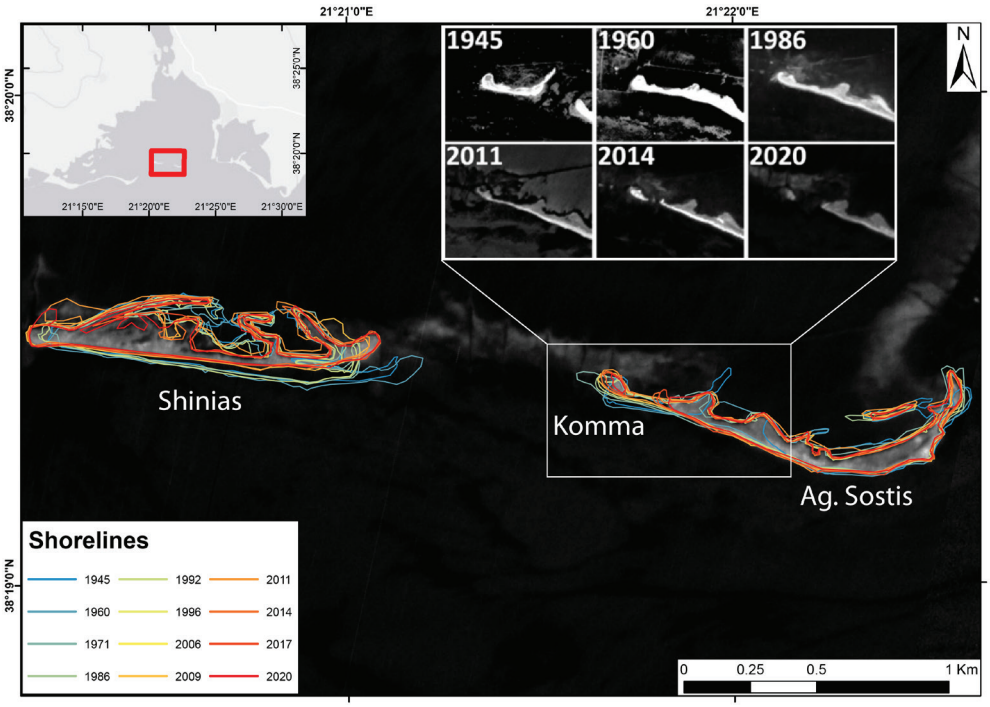

Fig. 9: Evolution of the Shinias islet area during 1945-2020 (km^2).

Comparative displacement of shorelines

Below is an example of the aforementioned detailed analysis and its results for the areas of Paleopotamos and Ekso Louros, at the central part of the broad study area. Considering the digitization accuracy, the following displacements are subject to an uncertainty of ±5 m.

Paleopotamos – Ekso Louros coastal areas

The area of Paleopotamos beach and Ekso Louros is approximately 10 km long and includes, from west to east, the mouth of Paleopotamos, a branch of the Acheloos river, which, in the past branched off between Koutsiliari and Skoupa hills and has now been cut off from the main route, the constructions for the containment of the estuary and further east the Ekso Louros cuspate foreland.

In the late 1970s and early 1980s, an artificial exit of the distributary to the Patraikos gulf in the South was opened, while between 1986 and 1992 the exit was entrenched, with vertical jetties, about 35 m long, on either side, at a distance of about 40 m between them (Fig. 11, circle 1). A second exit was also constructed approximately 1 km further east, which connected the Gouroupopoula lagoon with Patraikos gulf (Fig. 11, circle 2). By 1996 more parallel groins were built, covering an area of 1.5 km on either side of the Paleopotamos estuary.

Twelve coastlines, representatively covering the period 1945-2020, were digitized in the coastal area (Fig. 11). At first glance, the strong erosion can be observed in the western part of the sub-region, on either side of the Paleopotamos estuary, while no corresponding change is observed to the west, in the coastal area of Ekso Louros. It should be mentioned that in the areas where there are coastal works (jetties, groins, openings, etc.), the digitization of the coastline was done without considering the human constructions, but only the coastline, as it has been shaped due to the aforementioned works.

For the analysis of the area, 1047 transects perpendicular to the coastal were created, with a distance of 10 m between them (Fig. 12). Along each transect, at the point where the sections intersect, the movement of each year's coastlines was automatically calculated in relation to a baseline, common to all coastlines.

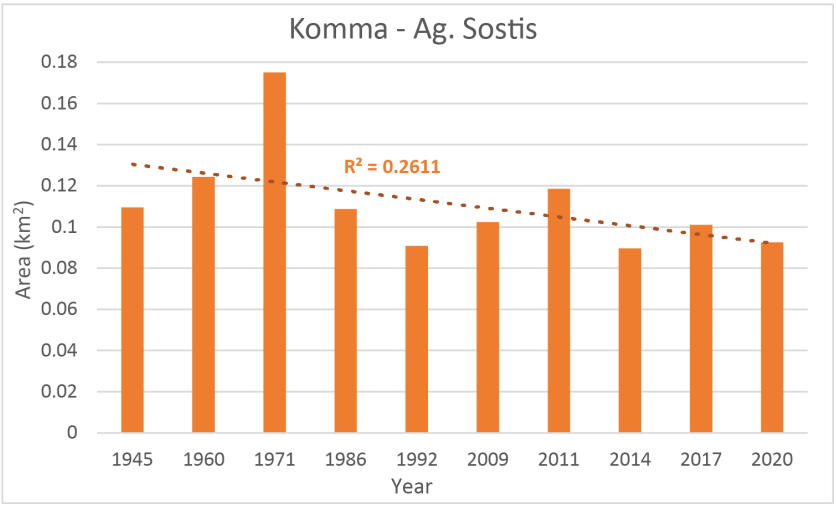

Fig. 10: Evolution of the Komma and Agios Sostis islets' areas during 1945-2020 (km²).

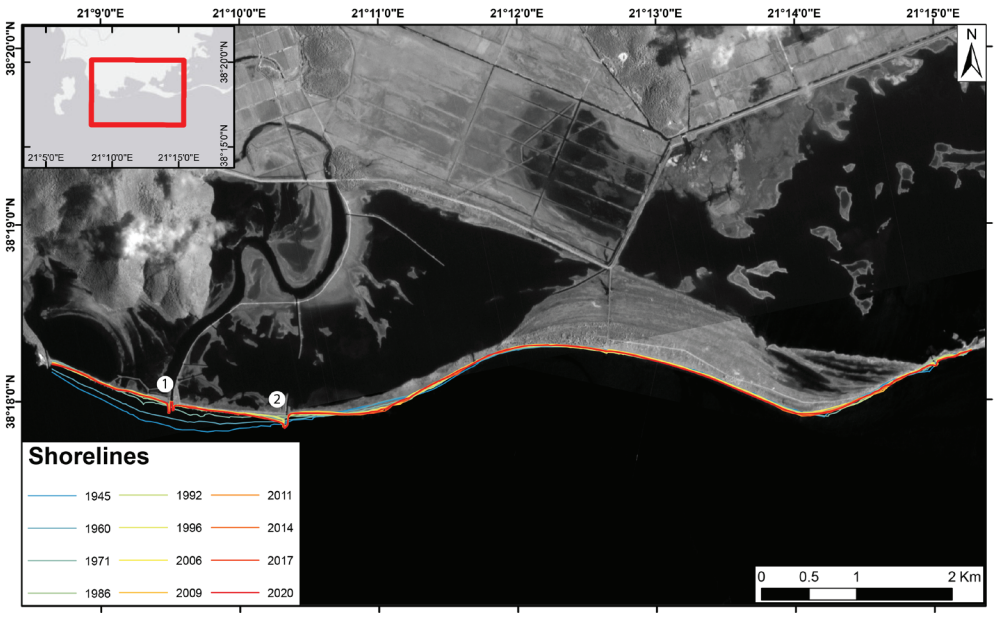

Fig. 11: Digitized shorelines of the study sub-area. Areas in circles 1 and 2 are described in the manuscript.

Net Shoreline Movement – NSM

As shown in Figure 12, the western part of the study area (sections 730-1047) has undergone significant erosion during the last 75 years. The advance observed in sections 773-777 is due to the artificial opening that joined the Gouronopoula lagoon with Patraikos gulf. Further east, advance is observed in the area of sections 632-727 and corresponding erosion in the immediately following section (453-631), while from that point and further east, along the entire length of Ekso Louros, alternating areas with small-scale erosion and deposition are observed.

Of the total of 1047 sections that form the study sub-area, 583 (55.7%) show retreat and 464 (44.3%) advance. The average shoreline displacement, based on all transects, is 42.5 m of retreating shoreline, while considering only transects in which retreat is observed, the corresponding mean value is -93.9 m. Maximum retreats are observed in the western part of the area (transects 855-960), with the extreme retreat observed at section 933, where the shoreline has retreated by 252.2 m. Accordingly, considering only the sections in which there is advance, the average value is 22 m. Maximum advance is observed in the central part of the area (transects 655-680), with the maximum advance observed at section 662, where the shoreline has advanced by 77.7 m.

End Point Rate – EPR

Figure 13 shows the average displacement rate for the study sub-area, which is -0.6 m/yr. Considering only the sections in which retreat is observed, the average retreat rate is -1.26 m/yr. The maximum retreat rate observed is 3.4 m/yr, at section 933, while it is equally high throughout the western part of the area (transects 855-960). The transects in which the advance of the coastline is observed have an average value of 0.3 m/yr and a maximum value of 1.1 m/yr.

Total Coastline Shift (1945-2020)

The coastal area eroded in the area that includes the Paleopotamos estuary and Ekso Louros, during the period 1945-2020, is approximately 0.551 km^2 (Fig. 14). The largest part of the lost area is in the coastal area of Paleopotamos, and the erosion is mainly found during the period 1945-1986. The construction of coastal protection works in the early 1980s succeeded in significantly halting erosion. The material deposit is located in the section between the estuary area and Ekso Louros and has an area of 0.094 km^2. The advance is due to the hydrodynamic regime, as there are no coastal constructions in this area. In the coastal area of Ekso Louros there is no significant change in the coastal area, with the exception of small local changes. The overall balance is negative, with an area loss of approximately 0.416 km^2 and it is by far the most important change in the wider area of the Acheloos delta.

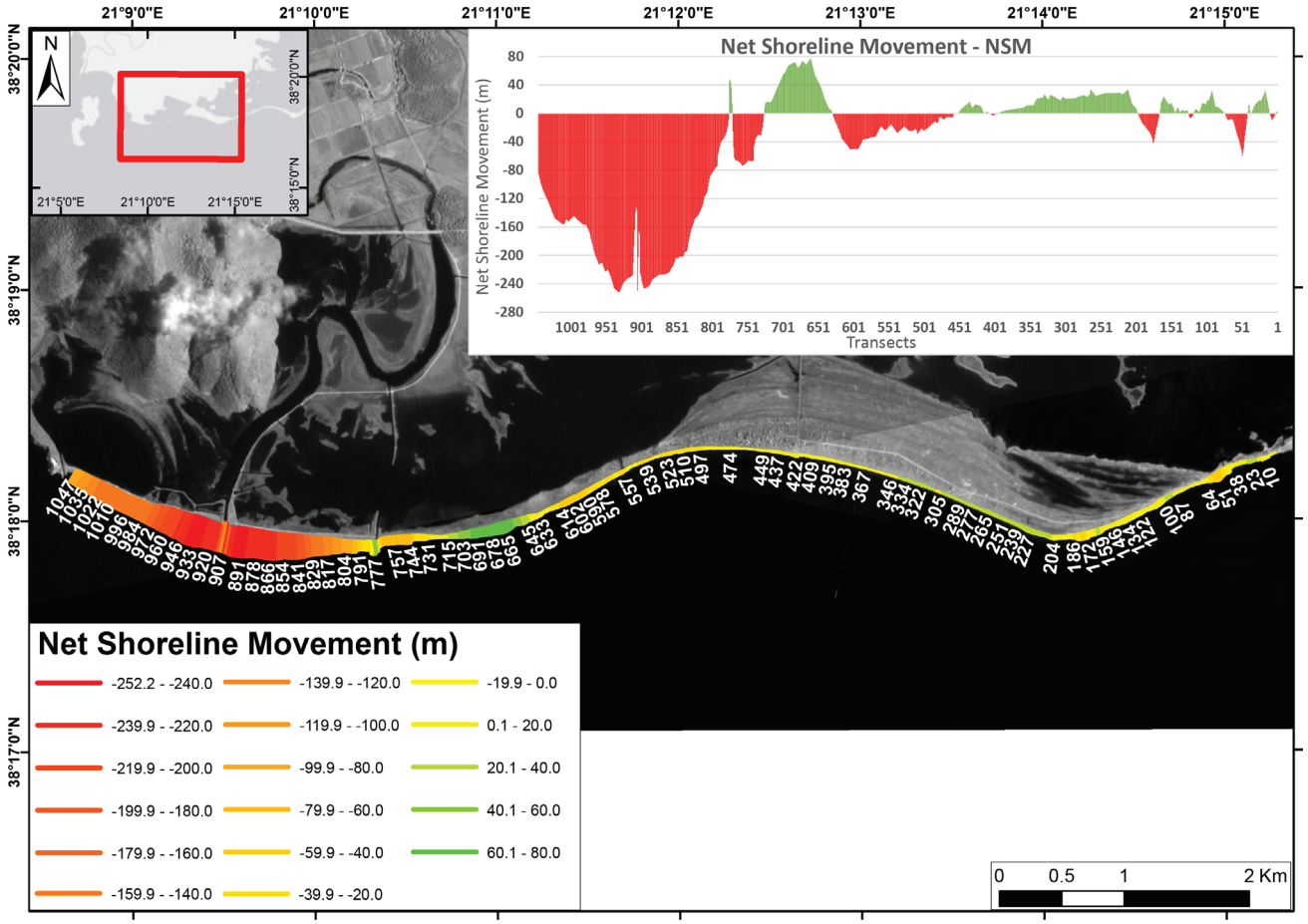

Fig. 12: Schematic representation of the Net Shoreline Movement (in m) at the study sub-area during the period 1945 – 2020.

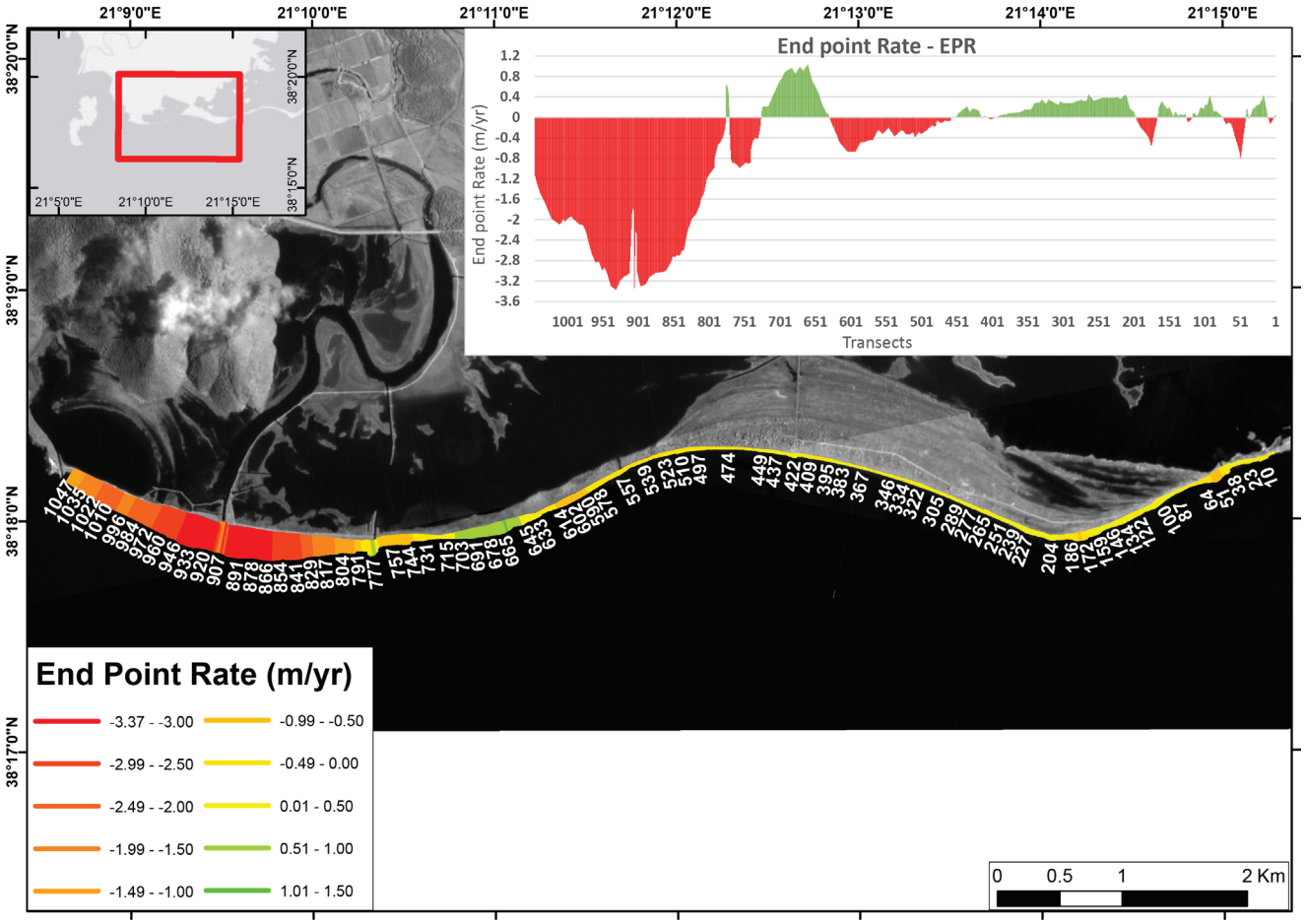

Fig. 13: Schematic representation of the End Point Rate (in m) at the study sub-area during the period 1945 – 2020.

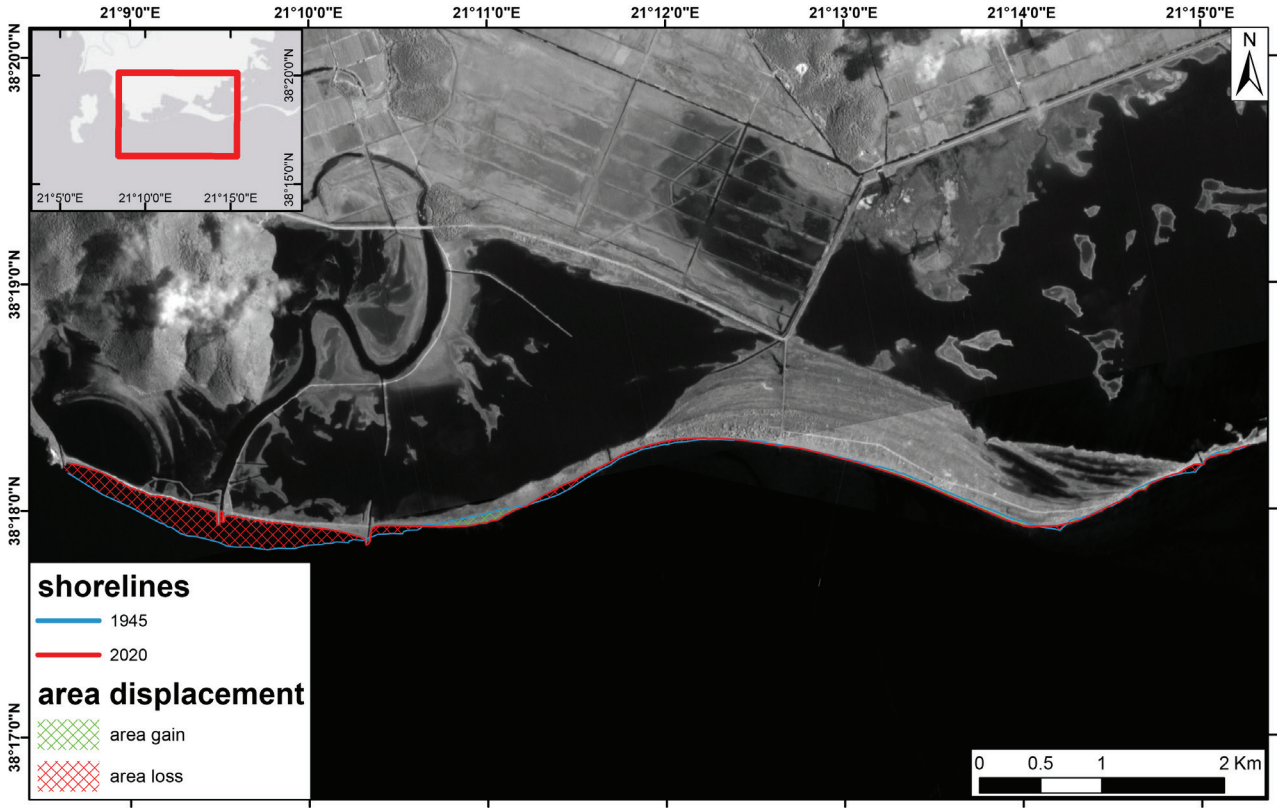

Fig. 14: Total alteration of the Paleopotamos – Ekso Louros area during 1945-2020.

Cumulative results of shorelines shifting

The same procedure as that analyzed for area 2 (Fig. 5) was followed for the rest of the areas. Figure 15 and Figure 17 show the consolidated map with all the areas in which the analysis of the long-term change and the rate of displacement of the coastline took place in the period 1945-2020, with the indicative colors of movements and rates being reduced to a common one for all areas to scale so that DSAS results can be compared between all study areas. Accordingly, in Figure 16 and Figure 18, the diagrams of the analyzes are presented.

The total number of transects created to study the evolution of the entire coastal front under consideration was 1743, with the majority of them belonging to sub-area 2. Of the 1743 transects, 1042 (59.8%) are subject to retreat, while in 700 sections (40.2%) an advance of the coastline is observed.

Cumulative Net Shoreline Movement – NSM

The average shoreline change for the entire study area is a retreat of 34.5 m over the past 75 years. Considering only the sections where retreat is observed, the average setback is 81.2 m. The area with the maximum values of the shoreline change over time is area 2 (Paleopotamos beach and Ekso Louros) and more specifically the

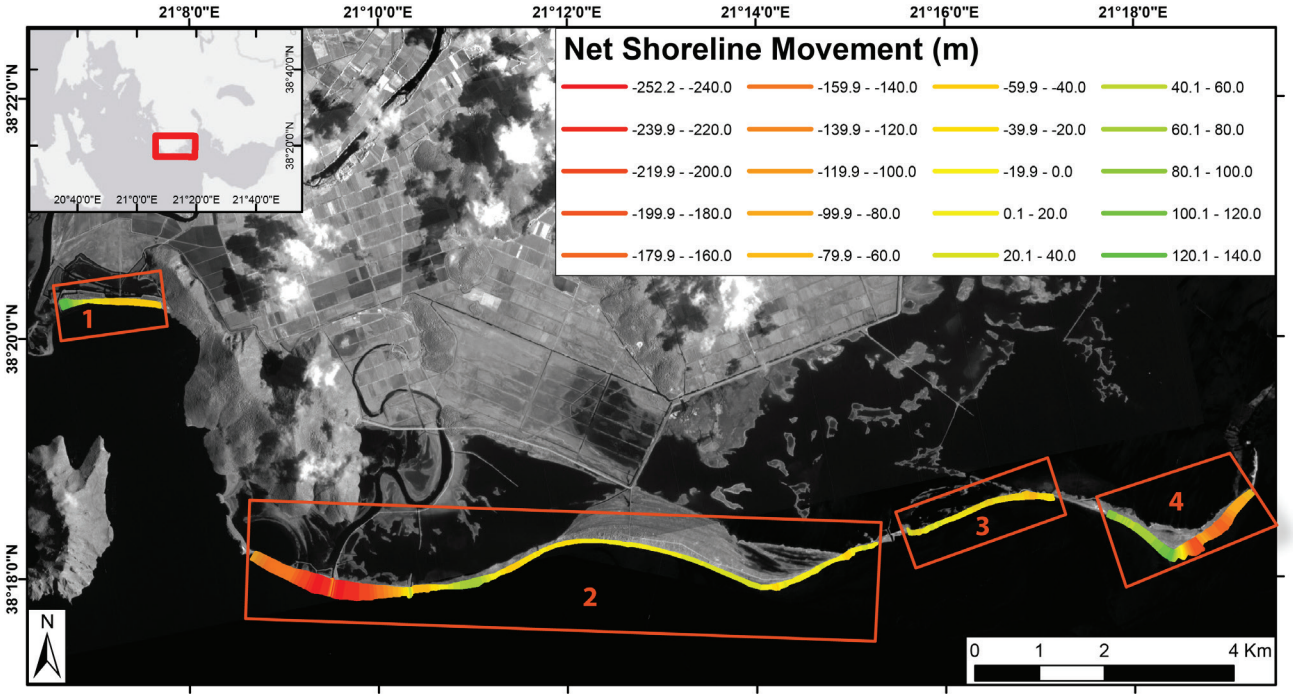

Fig. 15: Cumulative results of net shoreline displacement (in m) over time, for the period 1945 – 2020.

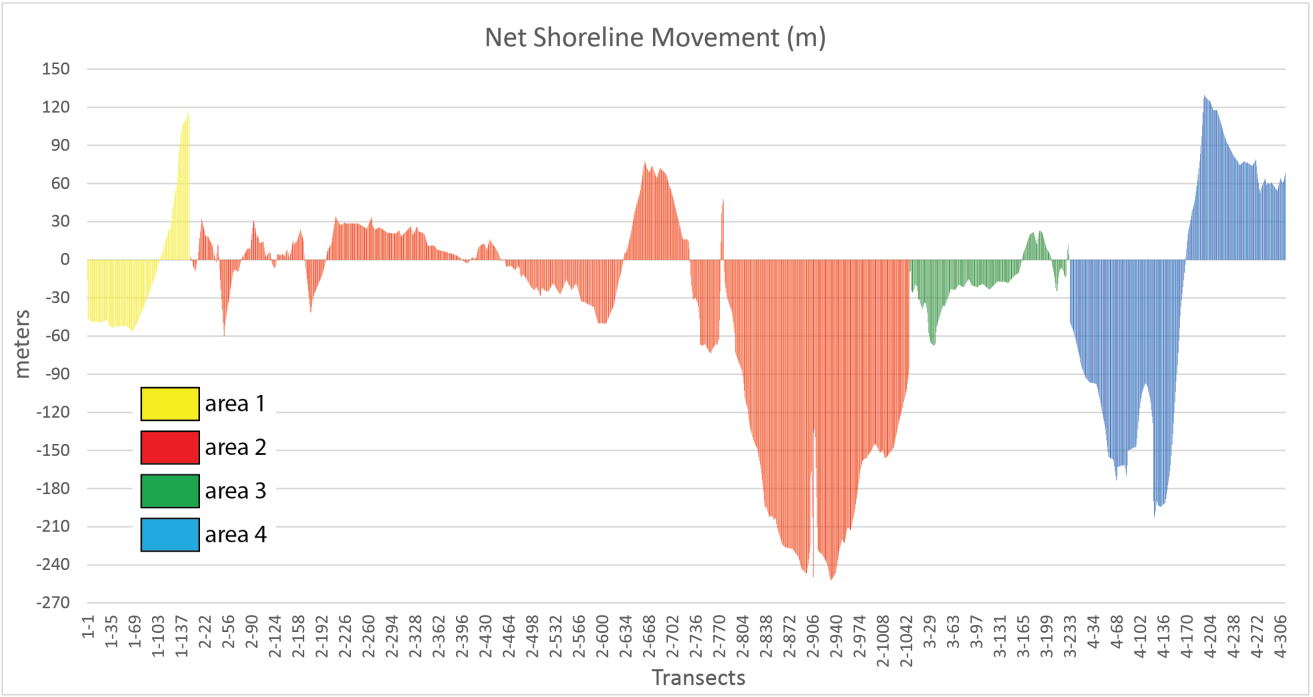

Fig. 16: Cumulative diagram of net shoreline displacement over time, for the total of the study area.

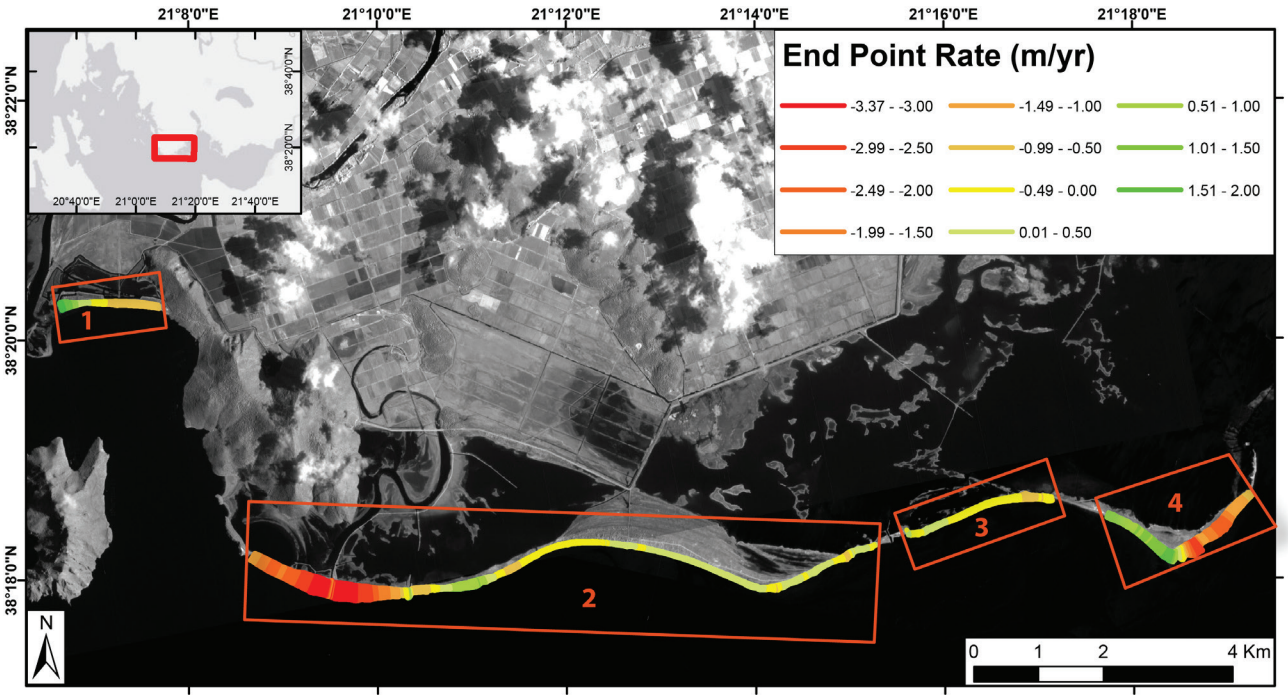

Fig. 17: Cumulative results of end point rate (m/yr) for the total of the study area, during the period 1945 – 2020.

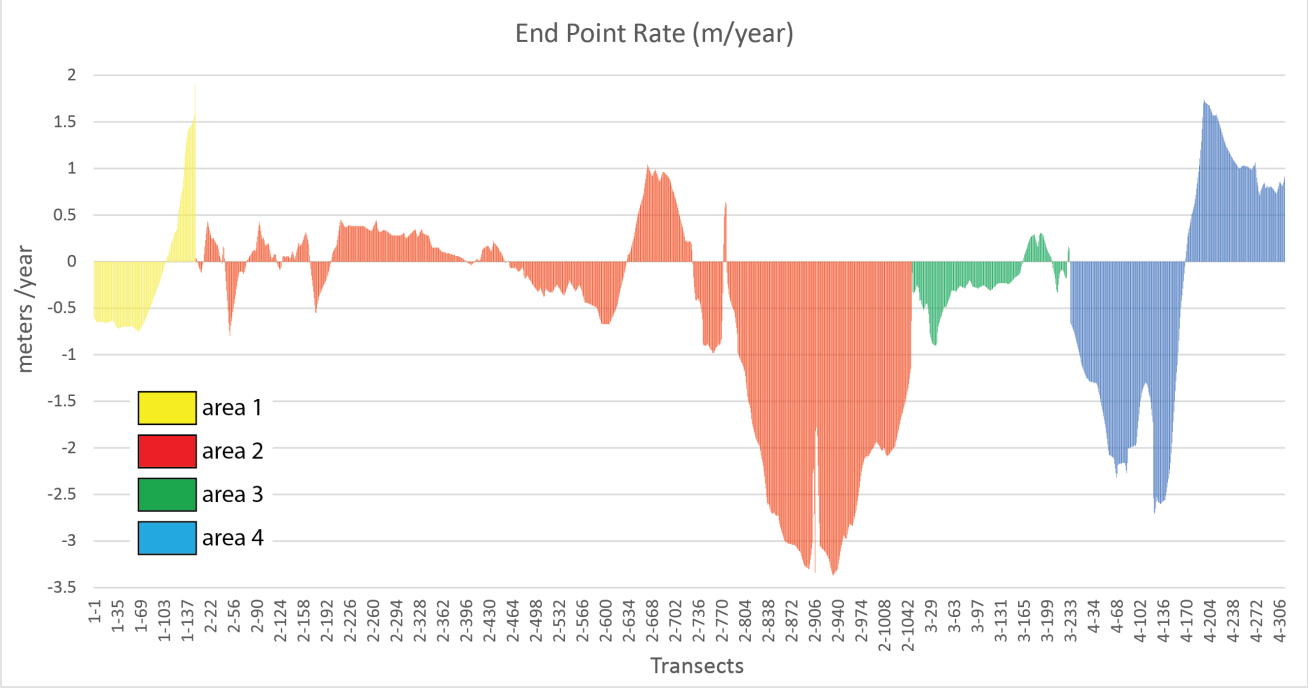

Fig. 18: Cumulative diagram of end point rate for the total of the study area.

western part, Paleopotamos beach. The maximum value of longitudinal retreat observed is 252.24 m and occurs at transect 933 of area 2, at the location of the Paleopotamos estuary.

In contrast, considering the sections along which advance is observed, the average for the entire study area is 35.14 m. The maximum advance is 129.9 m at transect 196 of area 4, on the western side of the southern end of Prokopanistos.

Cumulative End Point Rate – EPR

Of the total of 1743 sections plotted, the transects along which the displacement rate is negative (retreat) are 1037 (59.5% of the total), whereas the transects along which the displacement rate is positive (advance) are 695 (39.9%). In 11 transects (0.6% rate) the displacement rate is negligible. The average rate of shoreline displacement for the period 1945-2020, taking into account both retreating and advancing transects, is 0.46 m of retreat per year. Considering only the transects where shoreline retreat is observed, the average retreat is 1.09 m/yr. The maximum subsidence rate is located at transect 933 of sub-area 2, at the mouth of Paleopotamos and was estimated at 3.37 m/yr. Regarding the transects along which shoreline advance is observed, the average rate of advance is 0.47 m/yr, while the maximum value, 1.91 m/yr,

is located at transect 149 of sub-area 1, in the western part of the beach of Scrofa, just east of the modern estuary of Acheloos river.

In conclusion, almost the entire study area is under erosional regime. Coastal groines constructed in the western part of area 2 during the late 1970s and early 1980s and along the whole of area 3 between 1992-1996 have halted erosion to some extent, while in some parts advance of coastline was observed. In areas where there are no coastal works, erosion continues to this day, with minor exceptions due to the local hydrodynamic regime favoring local sections, through coastal sediment transport and deposition of material there.

The shoreline displacement values, both in the areas of erosion and in those where advance is observed, are comparable to the corresponding values analyzed in works for other deltas of Greece and the Mediterranean.

Indicatively in the Greek area, for the deltas of Aliakmonas and Axios (Northern Greece) and the period 1984-2009, the coastal delta area has lost 0.6 km^2 and 1.3 km^2, respectively (Petropoulos *et al.*, 2015). The Alfios delta has been receding at a rate of 8 m/yr up to 26.5 m/y, due to the construction of dams in its main route, since 1954 (Ghionis *et al.*, 2013; Poulos *et al.*, 2002). In the Arachthos delta that discharges into the Amvrakikos gulf, the total observed retreat is of the order of 20 m (Mertzanis & Mertzani, 2019), the Evinos delta shows retreats of 5 to 14 m/yr, mostly due to anthropogenic activities at the coast (Karymbalis *et al.*, 2022), while Nestos, whose deltaic plain is similar in size to that of Acheloos, shows an advance of its deltaic field during the period 1945-2002, at a rate of ~4 m/y, in contrast to the period 2002-2007, in which, due to the construction of dams, areas with advance and erosion of the order of 10 m/y are observed for both cases (Andredaki *et al.*, 2014). Pinios delta, with a deltaic plain area much smaller than that of Acheloos, has had a relatively similar rate of erosion since 1945, of the order of 3-4 m/y (Karymbalis *et al.*, 2016), while the Lilas delta in Evia island shows much lower erosion rates, <1 m/y (Karymbalis *et al.*, 2018).

Regarding the comparison with the major Mediterranean deltas, it is observed that, with the exception of the Nile, the retreats of the deltaic areas are of the same order as those measured in Acheloos. For example, Po delta in Italy, after the advance observed until 1954, is now retreating at a rate of about 10 m/y (Cencini, 1998). Also in Italy, the Marga River delta has been retreating at a rate of < 5 m/y over the last 130 years (Pratellesi *et al.*, 2018). At similar retreat rates (3–8 m/y) is the Rhone river delta in France (Sabatier *et al.*, 2009), while the Danube (Romania – Ukraine) and Guadalfeo (Spain) river deltas show higher retreat rates, 40 m /y and 16-20 m/y, respectively (Bergillos *et al.*, 2016; Romanescu, 2013).

In contrast, no comparison can be applied to the great world deltas, firstly because of the much larger area of both their watershed and the deltaic plain, and secondly because in these great deltas there is no homogeneity in deltaic shoreline displacement, as areas with significant retreat and areas with equally significant advance coexist in the same delta. For example, in the Ganges-Brahmaputra delta retreats of the order of 120 m/y and advances of the order of 230 m/y are observed (Matin & Hasan, 2021) and in the Yellow River of China retreats at a rate >180 m/y and advances >600 m/y (Fu *et al.*, 2021). An exception is the Mekong River delta in Vietnam, in which up to 2005 an advance was observed at a rate of ~5 m/y, followed by a retreat of the order of 1.4 m/y after 2005 (Liu *et al.*, 2017).

Implications of Future Sea Level Rise Due to Climate Change

The coastal area of Acheloos' delta, as mentioned earlier, is one of the highly vulnerable coastal areas of Greece, in terms of the immediate effects due to sea level rise. The coastal deltaic plain covers an area of about 80 km^2, with generally very small slopes (~0.1%), with the exception of the nearby coast hills (Koutsiliaris, Skoupas, Taksiarhis, etc.). Thus, a small sea level rise may result in the flooding of large areas of the deltaic plain. The smooth and low relief of the deltaic plain is depicted in the images of Figure 19, taken by drone from the area of Ekso Louros in the central section of the study area, and from the modern estuary of Acheloos, in the years 2019 and 2021 respectively.

As can be observed, the coastal area of Ekso Louros consists of semi-flooded areas of sclerophyllous vegetation and marshes, while deeper inland there are extensive areas of rice fields. The largest part of the modern Acheloos estuary consists of sandy, constantly moving areas, with temporary vegetation and an also very smooth morphology.

To predict the surface loss of the studied area beaches until the year 2100, an analysis of the existing situation was made, and the predictive models of the Intergovernmental Panel on Climate Change (IPCC) were applied to the aforementioned coasts (H.-O. Pörtner *et al.*, 2019).

The results of the analysis of sea level change data, based on the four different scenarios analyzed in chapter 4.2, are shown in Table 2 and Figure 20.

In order to have a measure of comparison in relation to the impact of sea level rise in the study area, Figure 21-a presents a morphological map of the wider area based on a detailed DTM with a 5 m resolution from the Greek Cadstre from 2015. The areas within the coastline of the study area (black line in the figure) which appear in dark red (like the one in the area of the Gouronopoula lagoon), are marshy parts, which are however cut off from the Messolonghi lagoon in the East, as well as from Outer Patraikos gulf in the South. The total land area shown in the image, with the exception of the Oxia islet in the Southwest, is 101 km^2, which is considered as the "base" for the study of the sea level rise.

Below are presented the effects that sea level rise will cause to the study area, according to the mean (0.50) confidence interval for each of the four different studied scenarios. Considering the DTM accuracy, the following flooding areas are subject to an uncertainty of ±25 m^2. It should be noted that the subsidence due to compaction

Fig. 19: General aerial views of the Acheloos estuary. Upper images: Ekso Louros and surrounding areas; Lower image: Modern estuaries. Images courtesy of A. Koutsothanasis.

Table 2. Sea level rise (m) for the study area based on various IPCC scenarios.

Year	RCP2.6 (very stringent)						
	0.05	0.17	0.50	0.84	0.95	0.99	StDv (±)
2010	0.02	0.03	**0.04**	0.05	0.06	0.07	0.02
2020	0.04	0.06	**0.08**	0.10	0.12	0.13	0.03
2030	0.07	0.09	**0.12**	0.15	0.18	0.21	0.05
2040	0.09	0.12	**0.16**	0.21	0.24	0.27	0.07
2050	**0.10**	**0.15**	**0.21**	**0.26**	**0.31**	**0.36**	0.10
2060	0.13	0.18	**0.26**	0.33	0.37	0.44	0.12
2070	0.13	0.20	**0.29**	0.38	0.44	0.50	0.14
2080	0.13	0.23	**0.33**	0.44	0.53	0.60	0.18
2090	0.14	0.24	**0.37**	0.49	0.59	0.70	0.21
2100	0.14	0.26	**0.41**	0.54	0.64	0.79	0.24
2020-2100	0.09	0.20	0.33	0.44	0.52	0.66	0.21

Year	RCP4.5 (stabilization)						
	0.05	0.17	0.50	0.84	0.95	0.99	StDv
2010	0.02	0.03	**0.04**	0.06	0.06	0.07	0.02
2020	0.04	0.06	**0.08**	0.10	0.12	0.13	0.03
2030	0.07	0.09	**0.12**	0.15	0.17	0.20	0.05
2040	0.09	0.13	**0.17**	0.21	0.25	0.28	0.07
2050	**0.11**	**0.16**	**0.22**	**0.28**	**0.32**	**0.37**	0.10
2060	0.15	0.20	**0.28**	0.36	0.42	0.47	0.13
2070	0.16	0.23	**0.33**	0.41	0.49	0.57	0.16
2080	0.19	0.29	**0.39**	0.51	0.60	0.72	0.20
2090	0.20	0.31	**0.45**	0.59	0.69	0.80	0.23
2100	0.22	0.35	**0.50**	0.67	0.79	0.96	0.28
2020-2100	0.18	0.28	0.42	0.56	0.68	0.82	0.24

Year	RCP8.5 (business as usual or baseline						
	0.05	0.17	0.50	0.84	0.95	0.99	StDv
2010	0.02	0.03	**0.04**	0.06	0.07	0.08	0.02
2020	0.05	0.06	**0.08**	0.10	0.12	0.14	0.03
2030	0.07	0.09	**0.13**	0.16	0.19	0.21	0.05
2040	0.10	0.14	**0.18**	0.23	0.27	0.31	0.08
2050	**0.14**	**0.19**	**0.25**	**0.32**	**0.36**	**0.42**	0.11
2060	0.17	0.23	**0.32**	0.40	0.46	0.53	0.14
2070	0.22	0.29	**0.40**	0.51	0.60	0.68	0.18
2080	0.25	0.36	**0.49**	0.62	0.74	0.83	0.23
2090	0.32	0.43	**0.59**	0.74	0.86	1.03	0.27
2100	0.35	0.49	**0.69**	0.87	1.03	1.20	0.33
2020-2100	0.30	0.43	0.60	0.77	0.91	1.06	0.29

Year	RCP8.5 Upper (worst)						
	0.05	0.17	0.50	0.84	0.95	0.99	StDv
2010	0.02	0.03	**0.04**	0.05	0.06	0.07	0.02
2020	0.06	0.07	**0.08**	0.10	0.11	0.13	0.03
2030	0.09	0.10	**0.13**	0.17	0.19	0.24	0.06
2040	0.12	0.15	**0.20**	0.26	0.32	0.40	0.11
2050	**0.17**	**0.21**	**0.28**	**0.38**	**0.47**	**0.58**	0.16
2060	0.21	0.27	**0.36**	0.49	0.69	0.88	0.26
2070	0.26	0.34	**0.46**	0.67	0.93	1.26	0.38
2080	0.33	0.41	**0.56**	0.84	1.15	1.65	0.51
2090	0.39	0.50	**0.69**	1.02	1.45	2.19	0.68
2100	0.45	0.58	**0.79**	1.21	1.92	2.69	0.87
2020-2100	0.39	0.51	0.71	1.11	1.81	2.56	0.85

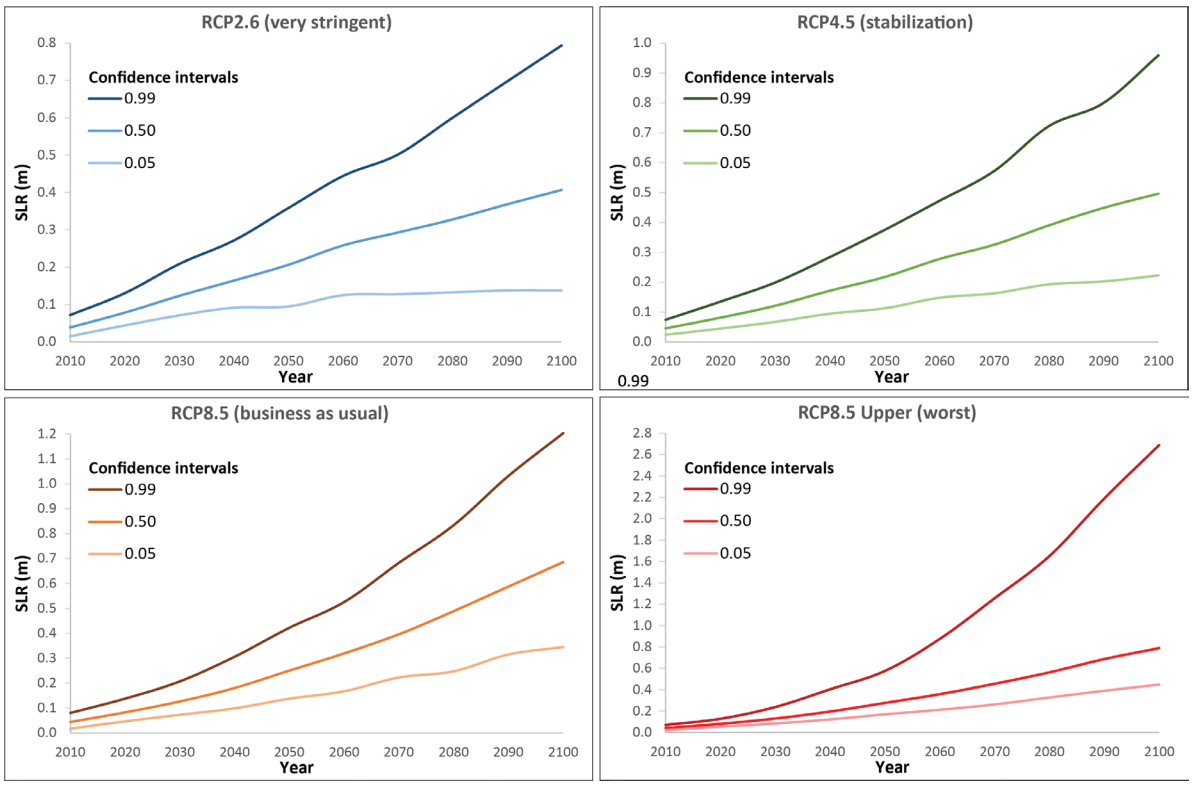

Fig. 20: Sea level rise confidence intervals, based on various IPCC scenarios, and 0.05, 0.50 and 0.90 confidence intervals.

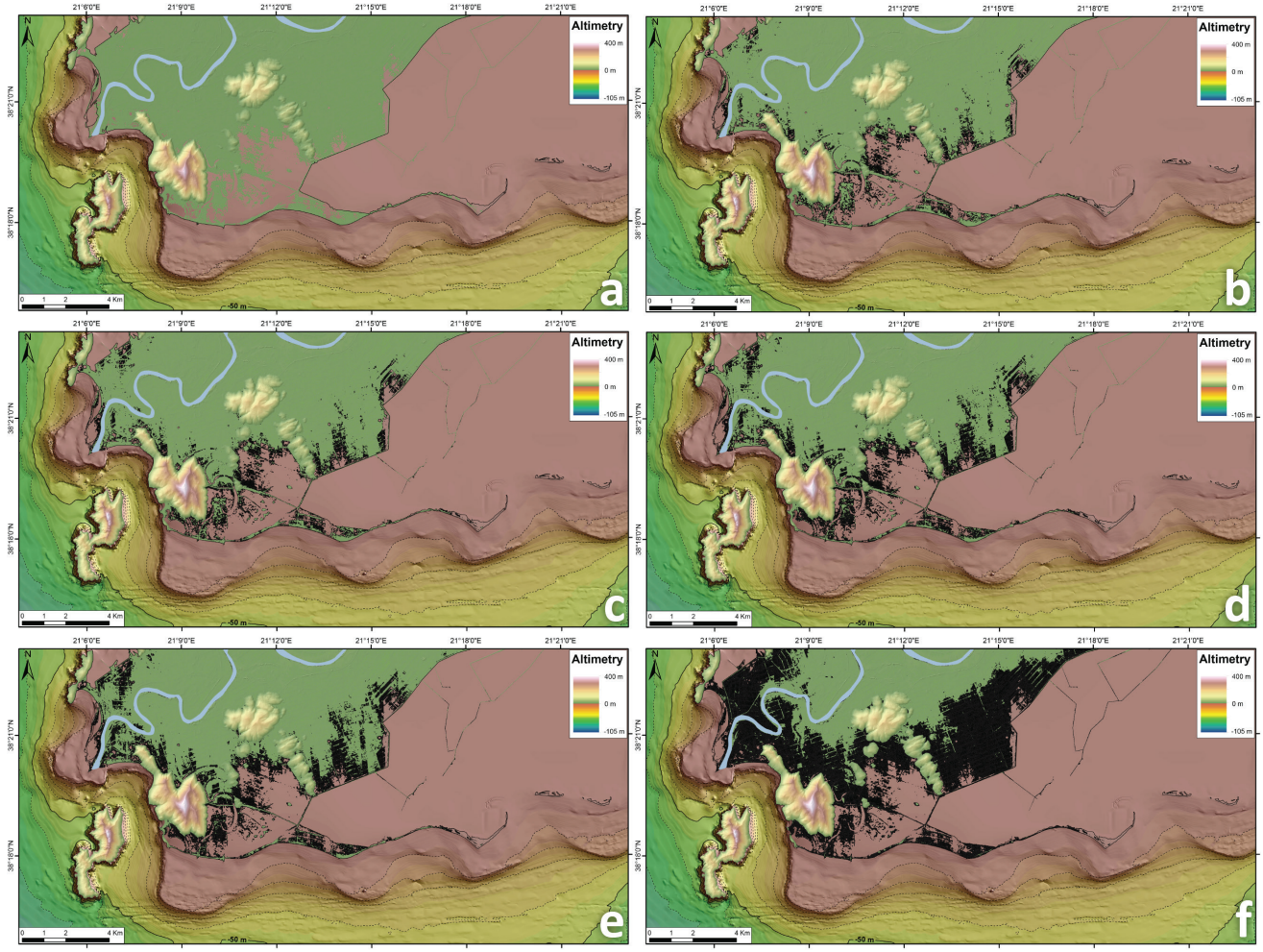

Fig. 21: The study area according to the RCP scenarios (flooded areas in black). (a) present topography, (b) SLR of 0.33m – RCP2.6, (c) SLR of 0.42m – RCP4.5 and RCP6, (d) SLR of 0.60m – RCP8.5, (e) SLR of 0.71m – High-end RCP8.5, (f) SLR of 1.81 m – High-end RCP8.5 with a confidence interval of 95%.

of the deltaic sediments and/or anthropogenic activities was not taken into consideration, due to lack of analogous information, though this component should not be of importance since the added sediment is very limited due to the aforementioned retention by the upstream dams.

RCP2.6 scenario

The results from the consideration of scenario RCP2.6 (very moderate), in which greenhouse gas emissions will decrease continuously and at a relatively fast rate until 2100, the global sea level rise for 2100 will be 0.26 to 0.55 m, with reference period of 1985-2000. In the study area, as shown in Table 2 and the graph in Figure 21-b, the expected rise is 0.41 m, while according to the 0.05 and 0.99 confidence intervals, it ranges from 0.14 to 0.79 m. With regard to the change in sea level in the period 2020-2100, i.e. removing the rise of the period 2010-2020, an average rise of 0.33 m is observed.

Figure 21-b shows the impact of this increase on the study area. In dark red (within the coastline) are the current semi-flooded areas, while in black are the areas that will be covered by water due to the above-mentioned rise in sea level. The area which remains unflooded was measured to be 91.64 km^2. Thus, it is observed that due to the rise of the water level by 0.33 m, the delta loses 9.36 km^2, or 9.3% of the total deltaic area. For spatial comparison, the area lost due to this increase is equivalent to the area occupied by the nearby city of Agrinio and its suburbs.

RCP4.5 scenario

Scenario RCP4.5 (moderate) projects greenhouse gas emissions to decrease slightly and at a slow rate until 2100. According to this scenario, the average global sea level rise is estimated to range between 0.32 and 0.63 m for the period 2010-2100. It is noted that the same rise values are given by Scenario RCP6, which predicts the emission of greenhouse gases to increase gradually, so it is considered that the impact on the study area for both of these scenarios is similar and thus is considered jointly. As shown in Table 2, the sea-level rise under the above-mentioned scenarios for the period 2010-2100 is 0.50 m, with confidence intervals giving a rise of 0.22 to 0.96 m. Excluding the first decade of the 21st century, the rise in 2100 relative to the present is 0.42 m. Figure 21-c shows the condition of the study area according to the rise resulting from the aforementioned scenarios. The total area covered by land is 89.59 km^2, which in relation to the present is reduced by 11.41 km^2, while compared to the very moderate scenario RCP2.6 it shows an additional 2.06 km^2 loss. The areas most affected in relation to the overall effect of the sea level rise are mainly in Paleopotamos and in the Western part of the Messolonghi lagoon, where the majority of the rice fields in the study area are located. A relatively large part of Ekso Louros and a small part of Prokopanistos are still above sea level, but parts of them have been submerged, leaving multiple passageways for the sea to the deltaic area.

RCP8.5 scenario

RCP8.5 Scenario (weighted extreme, but very possible scenario according to current scientific data), predicts a continued increase in greenhouse gas emissions until 2100 and high atmospheric pollution. Under this scenario, global average sea level rise will reach from 0.45 to 0.82 m by 2100. For the study area, the corresponding change for the period 2010–2100 is 0.69 m, with confidence intervals ranging between 0.35 and 1.20 m (Table 2). Excluding the decade 2010-2020 that has already passed, the sea level in 2100 will rise by 0.60 m relative to present level. Figure 21-d shows the study area with this sea level rise. The remaining deltaic area is 84.58 km^2, with a loss of 16.42 km^2, 16.3% of its current area.

High-End Scenario RCP8.5

The High-End Scenario RCP8.5 (extreme scenario, with greenhouse gas emission values like those of RCP8.5, but with an increased contribution of additional water from the melting of large ice stocks, mainly from Greenland and the Arctic), gives an average rise of global sea level by 0.80 m by 2100, while the 95% confidence interval (with a probability of 5%) gives a concerning global rise of 1.80 m (Jackson & Jevrejeva, 2016). For the study area, according to Table 2, for the period 2020-2100, the SL rise reaches an average of 0.71 m, ranging from 0.39 up to 2.56 m. Figure 21-e shows the impact of the SL rise for the 50% confidence interval in the study area. The area lost due to a 0.71 m SL rise is 19.8 km^2, equivalent to 19.6% of the total area of the deltaic plain in 2020, about 4 km^2 more than the lost area according to the RCP8.5 scenario.

High-End Scenario RCP8.5 (95%)

In order to have an overall picture of the impact of sea level rise in the region, the rise resulting from the 95% confidence interval (5% probability of being true) of the High-end RCP8.5 scenario was also studied, according to which the SL will rise by 1.81 m in the period 2020-2100 (Table 5-1). Obviously, the probability of this scenario being valid is rather small, just 5%, but it is also worth analyzing, due to the multifactorial nature of sea level change prediction models. Figure 21-f shows the state of the delta region with the sea level having risen by 1.81 m. The land surface in 2100 will have an area of 39.9 km^2, having lost 60.5% of the surface in 2020, i.e. 61.10 km^2, an area which is roughly equivalent to the current area of the Messolonghi lagoon. More specifically, the hills of Dioni, Koutsiliaris, Mikro – Megalo Vouni, Aspri Petra – Taxiarchis and Mavronisi have been cut off from the terrestrial deltaic surface, while Skoupas hill is half in contact with the coastline. The current deltaic area has receded by about 5 km, reaching the height of the southern part of Skoupas. Present Louronisides of the coastal area, as well as Ag. Sostis and Shinias in the southern part of

the Messolonghi lagoon have been completely covered by the rise of the sea level.

As mentioned above, the projected sea level changes for 2100 have a significant impact on the Acheloos River deltaic plain. This effect is due to the very small slope of the entire deltaic area, so that a slight rise in sea level has an impact on the intrusion of the sea over a long distance, also due to the fact that the elongated spit and artificial dikes in the southern area do not have the same height throughout their length so as to block the entry of the sea into the deltaic plain. Table 3 presents the different SL increases according to the various scenarios, as well as the land loss due to these scenarios.

Depending on the scenario, land loss ranges from 9.3 km^2 for the very moderate scenario to 19.6 km^2 for the extreme but very possible scenario. Analyzing the deltaic land loss, it is observed that for the 50% confidence interval of all scenarios studied it follows a perfectly linear relationship with sea level rise. For every 0.1 m SLR, the corresponding land loss is on average 2.77 km^2. Figure 22 shows the SLR diagram for the study area during the period 2010-2100, according to the four examined scenarios, while the right part shows, in the form of a bar, the range of confidence intervals for each scenario.

The greatest relative change in deltaic surface loss is observed under the moderate RCP2.6 scenario, corresponding to a sea-level rise of 33 cm. In contrast, under the RCP4.5 and RCP8.5 scenarios, land loss increases approximately linearly, scaling directly with the magnitude of sea-level rise projected for each scenario.

Conclusions

As highlighted above, the Acheloos deltaic system is a very fragile environment in the essence of its vulnerability to the sea level change, mostly due to the flatness of its morphology. This is enhanced by the anthropogenic interference, mainly in the upstream river flow, with the construction of several dams that retain large amounts of sediment, as about 65% of the drainage basin has been cut off due to the dams. The result is clearly reflected in the coastal area, where large land retreats are observed, reaching in certain areas the 250 m for the last 75 years. The average retreat for this period is 35 m, while the total land loss is 1.63 km^2.

The estimated deltaic land loss due to the anticipated sea level rise by 2100, depending on the four main IPCC climate scenarios (RCP2.6, RCP4.5, RCP8.5 and High-End RCP8.5), is from 9.36 km^2 for the most mod-

Table 3. Cumulative board of the deltaic area alteration during the period 2020-2100, according to the various SLR scenarios.

	Scenarios					
	Present	**RCP2.6**	**RCP4.5**	**RCP8.5**	**High-end RCP8.5**	**High-end RCP8.5 (95%)**
Area (km^2)	101	91.64	89.59	84.58	81.20	39.90
SLR (m)	-	0.33	0.42	0.60	0.71	1.81
Land loss (km^2)	-	9.36	11.41	16.42	19.80	61.10
Loss percentage (%)	-	**9.3**	**11.3**	**16.3**	**19.6**	**60.5**

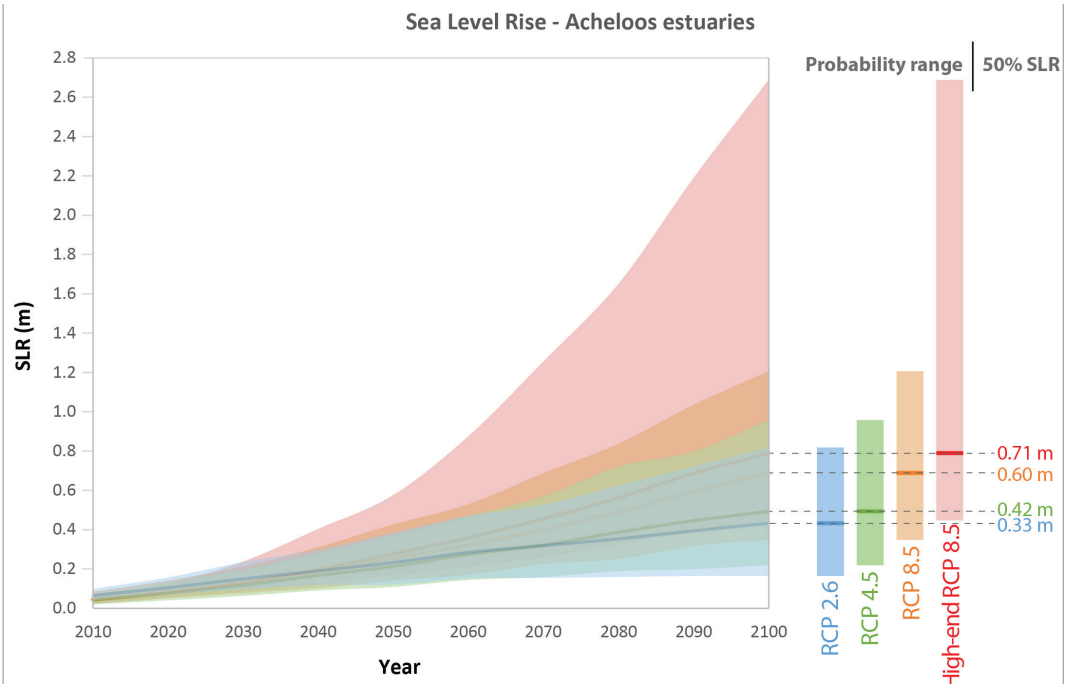

Fig. 22: Cumulative SLR diagram of the area for the period 2010-2100.

erate scenario, to 19.8 km^2 to the most extreme scenario. In general, it has been calculated that for every 0.1 m of SLR the average area loss is 2.77 km^2. The area that will be lost is currently occupied mostly by rice fields, and permanently (or partially) irrigated cultivations, that will result in a direct affect to the regional economy. Efforts are made to withhold the erosion with the construction of coastal protection works, although, as observed, a more inclusive management of the broad deltaic system has to be implemented, with focus on the sediment yield controlled by the dams upstream.

References

Alley, R.B., Clark, P.U., Huybrechts, P., Joughin, I., 2005. Ice-sheet and sea-level changes. *Science*, 310, 456–460.

Andredaki, M., Georgoulas, A., Hrissanthou, V., Kotsovinos, N., 2014. Assessment of reservoir sedimentation effect on coastal erosion in the case of Nestos River, Greece. *International Journal of Sediment Research*, 29 (1), 34–48.

Anthony, E.J., Besset, M., Zainescu, F., Sabatier, F., 2021. Multi-decadal deltaic land-surface changes: Gauging the vulnerability of a selection of Mediterranean and Black Sea river deltas. *Journal of Marine Science and Engineering*, 9 (5), 512.

Anthony, E.J., Dussouillez, P., Dolique, F., Besset, M., Brunier, G. *et al.*, 2017. Morphodynamics of an eroding beach and foredune in the Mekong River delta: Implications for deltaic shoreline change. *Continental Shelf Research*, 147, 155–164.

Bergillos, R.J., López-Ruiz, A., Ortega-Sánchez, M., Masselink, G., Losada, M.A., 2016. Implications of delta retreat on wave propagation and longshore sediment transport – Guadalfeo case study (southern Spain). *Marine Geology*, 382, 1–16.

Besset, M., Anthony, E.J., Bouchette, F., 2019. Multi-decadal variations in delta shorelines and their relationship to river sediment supply: An assessment and review. *Earth-Science Reviews*, 193, 199–219.

Besset, M., Anthony, E.J., Sabatier, F., 2017. River delta shoreline reworking and erosion in the Mediterranean and Black Seas: The potential roles of fluvial sediment starvation and other factors. *Elementa: Science of the Anthropocene*, 5, 54.

Calvin, K., Dasgupta, D., Krinner, G., Mukherji, A., Thorne, P.W., *et al.*, 2023. Climate Change 2023: Synthesis Report. Contribution of Working Groups I, II and III to the Sixth Assessment Report of the Intergovernmental Panel on Climate Change. *Intergovernmental Panel on Climate Change*, 35–115.

Cazcarro, I., Arto, I., Hazra, S., Bhattacharya, R.N., Adjei, P.O.W., *et al.*, 2018. Biophysical and socioeconomic state and links of deltaic areas vulnerable to climate change: Volta (Ghana), Mahanadi (India) and Ganges–Brahmaputra–Meghna (India and Bangladesh). *Sustainability*, 10 (3) 893.

Cencini, C., 1998. Physical processes and human activities in the evolution of the Po Delta, Italy. *Journal of Coastal Research*, 14, 774–793.

Dunn, F.E., Darby, S.E., Nicholls, R.J., Cohen, S., Zarfl, C., Fekete, B.M., 2019. Projections of declining fluvial sediment delivery to major deltas worldwide in response to climate change and anthropogenic stress. *Environmental Research Letters*, 14 (8), 084034.

Elliott, M., 2002. The role of the DPSIR approach and conceptual models in marine environmental management: An example for offshore wind power. *Marine Pollution Bulletin*, 44.

Fu, Y., Chen, S., Ji, H., Fan, Y., Li, P., 2021. The modern Yellow River Delta in transition: Causes and implications. *Marine Geology*, 436, 106476.

Galloway, W.E., 1975. Process framework for describing the morphologic and stratigraphic evolution of deltaic depositional systems. *Houston Geological Society*, 87–98.

Ghionis, G., Poulos, S.E., Karditsa, A., 2013. Deltaic coastline retreat due to dam construction: The case of the River Alfios mouth area (Kyparissiakos Gulf, Ionian Sea). *Journal of Coastal Research*, 165, 2119–2124.

Guneroglu, A., 2015. Coastal changes and land use alteration on northeastern part of Turkey. *Ocean and Coastal Management*, 118, 225–233.

Himmelstoss, E.A., Henderson, R.E., Kratzmann, M.G., Farris, A.S., 2018. Digital Shoreline Analysis System (DSAS) Version 5.0 User Guide. *United States Geological Survey Open-File Report*, 2018–1179, 1–126.

Hydrographic Service – Hellenic Navy, 2015. Sea Level Statistics of Greek Ports. *Hydrographic Service – Hellenic Navy.*

Jackson, L.P., Jevrejeva, S., 2016. A probabilistic approach to 21st century regional sea-level projections using RCP and High-end scenarios. *Global and Planetary Change*, 146, 179–189.

Jevrejeva, S., Jackson, L.P., Riva, R.E.M., Grinsted, A., Moore, J.C., 2016. Coastal sea level rise with warming above 2° C. *Proceedings of the National Academy of Sciences of the United States of America*, 113 (47), 13342–13347.

Kapsimalis, V., Poulos, S.E., Karageorgis, A.P., Pavlakis, P., Collins, M., 2005. Recent evolution of a Mediterranean deltaic coastal zone: Human impacts on the Inner Thermaikos Gulf, North Aegean Sea. *Journal of the Geological Society*, 162 (6), 897–908.

Karditsa, A., Tsapanou, A., Poulos, S.E., 2020. The evolution of the transboundary Evros River delta (Northeast Aegean Sea) under human intervention: A seven-decade analysis. *Physical Geography*, 41 (4) 291–314.

Karymbalis, E., 2010. Coastal Geomorphology. *ION Publications.*

Karymbalis, E., Gaki-Papanastassiou, K., Tsanakas, K., Ferentinou, M., 2016. Geomorphology of the Pinios River delta, Central Greece. *Journal of Maps*, 12 (sup. 1), 12–21.

Karymbalis, E., Gallousi, C., Cundy, A., Tsanakas, K., Gaki-Papanastassiou, K., *et al.*, 2022. Long-term spatial and temporal shoreline changes of the Evinos River delta, Gulf of Patras, Western Greece. *Zeitschrift für Geomorphologie*, 63 (2-3), 141–155.

Karymbalis, E., Valkanou, K., Tsodoulos, I., Iliopoulos, G., Tsanakas, K., *t al.*, 2018. Geomorphic evolution of the Lilas River fan delta (Central Evia Island, Greece). *Geosciences*, 8 (10), 1–16.

Kristensen, P., 2004. The DPSIR framework. *European Environment Agency*, 1–10.

Liu, P., DeMaster, D., Nguyen, T., Saito, Y., Nguyen, V.L. *et*

al., 2017. Stratigraphic formation of the Mekong River Delta and its recent shoreline changes. *Oceanography*, 30 (3), 72–83.

Ludwig, W., Dumont, E., Meybeck, M., Heussner, S., 2009. River discharges of water and nutrients to the Mediterranean and Black Sea: major drivers for ecosystem changes during past and future decades? *Progress in Oceanography*, 80 (3), 199–217.

Lykakis, N., De La Fuente, J.M., Gagala, L., Granado, P., Spanos, D. *et al.*, 2021. Application of salt outcrop studies to offshore seismic interpretation in Western Greece. In: *Third EAGE Eastern Mediterranean Workshop* (Vol. 2021, No. 1, pp. 1-3). European Association of Geoscientists & Engineers.

Matin, N., Hasan, G.M.J., 2021. A quantitative analysis of shoreline changes along the coast of Bangladesh using remote sensing and GIS techniques. *Catena*, 201, 105185.

Mertzanis, A., Mertzani, A., 2019. Climate change and man-made interventions as destabilizing factors of the coastal zone: Some examples of coasts and coastal wetlands in Greece. *International Journal of Environment and Climate Change*, 9 (11), 616–642.

Meyer, H., Peters, R., 2016. A plea for putting the issue of urbanizing deltas on the New Urban Agenda.

Milliman, J.D., Farnsworth, K.L., 2011. River discharge to the coastal ocean: A global synthesis. *Cambridge University Press.*

Nghiningwa, A.N., Adelekan, I.O., Mshelia, Z.H., 2025. Shoreline change, sea level rise and the impacts along the coastline of Walvis Bay, Namibia. *Ocean and Coastal Management*, 266, 107690.

National Oceanic and Atmospheric Administration (NOAA), 2012. Mapping Coastal Inundation Primer. *National Oceanic and Atmospheric Administration*, 1–28.

Ortega, A.Y., Otero Díaz, L.J., Cueto, J.E., 2023. Assessment and management of coastal erosion in the marine protected area of the Rosario Island archipelago (Colombian Caribbean). *Ocean and Coastal Management*, 239, 106605.

Papanikolaou, D.J., 2015. Geology of Greece. *Patakis Publications.*

Parcharidis, I., Kourkouli, P., Karymbalis, E., Foumelis, M., 2013. Time series synthetic aperture radar interferometry for ground deformation monitoring over a small-scale tectonically active deltaic environment (Mornos, Central Greece). *Journal of Coastal Research*, 29 (2), 325–338.

Petropoulos, G.P., Kalivas, D.P., Griffiths, H.M., Dimou, P.P., 2015. Remote sensing and GIS analysis for mapping spatio-temporal changes of erosion and deposition of two Mediterranean river deltas: The case of the Axios and Aliakmonas rivers, Greece. *International Journal of Applied Earth Observation and Geoinformation*, 35, 217–228.

Pörtner, H.-O., Masson-Delmotte, V., Zhai P., Tignor, M., Poloczanska, E. *et al.*, 2019. IPCC Special Report on the Ocean and Cryosphere in a Changing Climate. *Intergovernmental Panel on Climate Change.*

Poulos, S.E., 2019. River systems and their water and sediment fluxes towards the marine regions of the Mediterranean Sea and Black Sea Earth System: An overview. *Mediterranean Marine Science*, 20 (3), 549–565.

Poulos, S.E., Collins, M.B., 2002. Fluviatile sediment fluxes to the Mediterranean Sea: A quantitative approach and the influence of dams. *Geological Society Special Publications*, 191 (1), 227–245.

Poulos, S.E., Voulgaris, G., Kapsimalis, V., Collins, M., Evans, G., 2002. Sediment fluxes and the evolution of a riverine-supplied tectonically active coastal system: Kyparissiakos Gulf, Ionian Sea (Eastern Mediterranean). *Geological Society Special Publications*, 191, 247–266.

Pratellesi, M., Ciavola, P., Ivaldi, R., Anthony, E.J., Armaroli, C., 2018. River-mouth geomorphological changes over >130 years (1882–2014) in a small Mediterranean delta: Is the Magra delta reverting to an estuary? *Marine Geology*, 403, 215–224.

Rafi, S., Mourya, N.K., Balasani, R., 2024. Evaluation of shoreline alteration along the Jagatsinghpur District coast, India (1990–2020) using Digital Shoreline Analysis System (DSAS). *Ocean and Coastal Management*, 253, 107132.

Reader, M.O., Eppinga, M.B., de Boer, H.J., Damm, A., Petchey, O.L. *et al.*, 2022. The relationship between ecosystem services and human modification displays decoupling across global delta systems. *Communications Earth and Environment*, 3 (1) 102.

Romanescu, G., 2013. Alluvial transport processes and the impact of anthropogenic intervention on the Romanian littoral of the Danube Delta. *Ocean and Coastal Management*, 73, 31–43.

Sabatier, F., Samat, O., Ullmann, A., Suanez, S., 2009. Connecting large-scale coastal behaviour with coastal management of the Rhône delta. *Geomorphology*, 107 (1-2), 79–89.

Santos, M.J., Dekker, S.C., 2020. Locked-in and living delta pathways in the Anthropocene. *Scientific Reports*, 10 (1), 1–10.

Schmitt, R.J.P., Bizzi, S., Castelletti, A., Kondolf, G.M., 2018. Improved trade-offs of hydropower and sand connectivity by strategic dam planning in the Mekong. *Nature Sustainability*, 1 (2), 96–104.

Scown, M.W., Dunn, F.E., Dekker, S.C., van Vuuren, D.P., Karabil, S. *et al.*, 2023. Global change scenarios in coastal river deltas and their sustainable development implications. *Global Environmental Change*, 82, 102736.

Skoulikidis, N., 2016. The state and origin of river water composition in Greece. In *The Rivers of Greece: Evolution, Current Status and Perspectives* (pp. 97-127). Berlin, Heidelberg: Springer Berlin Heidelberg.

Soto, J.I. Tranos, M.D., Bega, Z., Dooley, T.P., Hernández, P. *et al.*, 2024. Contrasting styles of salt-tectonic processes in the Ionian Zone (Greece and Albania). *Tectonics*, 43, 1–46.

Soukisian, T., Hatzinaki, M., Korres, G., Papadopoulos, A., Kallos, G., 2007. Wind and wave atlas of the Hellenic Seas. *Hellenic Centre for Marine Research.*

Stathopoulou, A. Papatheodorou, G., Tripsanas, E., Ferrari, A.H., Rubi, R. *et al.*, 2023. Evolution of the low-stand Acheloos fluvial-dominated delta complex in Western Greece. *Proceedings of the EAGE Eastern Mediterranean Workshop.*

Syvitski, J., Ángel, J.R., Saito, Y., Overeem, I., Vörösmarty, C.J. *et al.*, 2022. Earth's sediment cycle during the Anthropocene. *Nature Reviews Earth and Environment*, 3 (3), 179–196.

Syvitski, J.P.M., Kettner, A.J., Overeem, I., Hutton, E.W.H.,

Hannon, M.T. *et al.*, 2009. Sinking deltas due to human activities. *Nature Geoscience*, 2, 681–686.

Tsokos, A., Kotsi, E., Petrakis, S., Vassilakis, E., 2018. Combining multi-source remote sensing datasets for shoreline displacement rates. *Journal of Coastal Conservation*, 22 (2), 431–441.

Tzanetatou, V., Ghionis, G., Ferentinos, G., 2002. Morphological evolution of the coastal zone of the Acheloos Delta. *Proceedings of the Panhellenic Geographical Congress*, 363–366.

Underhill, J.R., 1988. Triassic evaporites and Plio-Quaternary diapirism in Western Greece. *Journal of the Geological Society*, 145 (2), 269–282.

Vörösmarty, C.J., Meybeck, M., Fekete, B., Sharma, K., Green, P., *et al.*, 2003. Anthropogenic sediment retention: Major global impact from river impoundments. *Global and Planetary Change*, 39 (1-2), 169–190.